

## RESEARCH ARTICLE

10.1002/2017JC012928

## The Dynamics of Cuba Anticyclones (CubANs) and Interaction With the Loop Current/Florida Current System

Vassiliki Kourafalou<sup>1</sup> , Yannis Androulidakis<sup>1</sup>, Matthieu Le Hénaff<sup>2,3</sup> , and HeeSook Kang<sup>1</sup> 

## Key Points:

- Anticyclonic mesoscale eddies along Cuba (CubAN eddies) are identified and characterized for the first time
- The formation and evolution of CubAN eddies is strongly associated with the variability of the Loop Current/Florida Current system
- Wind-induced upwelling and cyclonic eddies along the northern Cuban coast influence the eastward propagation of CubAN eddies

## Correspondence to:

V. Kourafalou,  
vkourafalou@rsmas.miami.edu

## Citation:

Kourafalou, V., Androulidakis, Y., Le Hénaff, M., & Kang, H.S. (2017). The dynamics of Cuba Anticyclones (CubANs) and interaction with the Loop Current/Florida Current system. *Journal of Geophysical Research: Oceans*, 122, 7897–7923. <https://doi.org/10.1002/2017JC012928>

Received 28 MAR 2017

Accepted 6 SEP 2017

Accepted article online 14 SEP 2017

Published online 17 OCT 2017

<sup>1</sup>Department of Ocean Sciences, Rosenstiel School of Marine and Atmospheric Science, University of Miami, Miami, FL, USA, <sup>2</sup>Cooperative Institute for Marine and Atmospheric Studies, University of Miami, Miami, FL, USA, <sup>3</sup>NOAA/Atlantic Oceanographic and Meteorological Laboratory, Miami, FL, USA

**Abstract** Mesoscale anticyclonic eddies along the northern Cuban coast (CubANs) have been identified in the Straits of Florida, associated with the northward shift of the Florida Current (FC) and the anticyclonic curvature of the Loop Current (LC) at the western entrance of the Straits. The dynamics of CubAN eddies and their interaction with the LC/FC system are described for the first time using satellite, drifter and buoy data, and a high-resolution model. It is shown that the evolution of CubANs to the south of the FC front complements the evolution of cyclonic eddies to the north of the FC, advancing previous studies on synergy between FC meandering and eddy activity. Two types of CubAN eddies are characterized: (a) a main anticyclonic cell (type “A”) within the core of the LC during retracted phase conditions, associated with the process of LC Eddy (LCE) shedding from an extended LC, and (b) an individual, distinct anticyclonic eddy that is released from the main LC core and is advected eastward, along the northern Cuban coast (type “B”). There are also mixed cases, when the process of LCE shedding has started, so a type “A” CubAN is being formed, in the presence of one or more eastward progressing type “B” eddies. CubAN evolution is associated with an increased mixed layer and weaker stratification of the upper ocean along the eddy’s track. The cyclonic activity along the Cuban coast and wind-induced upwelling events also contribute to the evolution and fate of the CubAN eddies.

## 1. Introduction

### 1.1. Background

The connectivity between the Caribbean Sea and the Atlantic Ocean is controlled by the Gulf Stream system. Its manifestation in the Gulf of Mexico (GoM) is called the Loop Current (LC), and through the Straits of Florida it is called the Florida Current (FC). The southern part of the Straits of Florida is oriented in an east-west direction, constrained by narrow shelf areas along the northern Cuban coast in the south and the Florida Keys Reef Tract in the north (see Figure 1 for all locations mentioned in text). The Gulf Stream is a component of the Atlantic Meridional Overturning Circulation, which plays a key role in the global climate regulation and evolution (Srokosz & Bryden, 2015). Changes in the LC influence the downstream FC dynamics (Fratantoni et al., 1998; Lee et al., 1995), under a synergy between FC meandering and evolution of cyclonic eddies through the Straits of Florida (Fratantoni et al., 1998; Kourafalou & Kang, 2012; Lee et al., 1995; Le Hénaff et al., 2014). These processes are important for South Florida communities, as they have implications on socioeconomic issues associated with fisheries and tourism. In particular, coral reef health has been found to be influenced by local and regional connectivity processes that connect the undulations of the LC/FC system to coral fish larval transport (Sponaugle et al., 2005, 2012; Vaz et al., 2016).

We have identified a mechanism affecting the evolution of the LC/FC system, which has not been addressed in previous studies, namely the development and evolution of mesoscale anticyclonic eddies along northwestern Cuba, hereafter named CubAN eddies. The objective of this study is to investigate processes related to CubAN formation and progression, in tandem with their influence on both local (northern Cuba) and basin-wide (GoM) dynamics. In particular, we aim to explore to what extent CubAN eddies, either at the base of the LC core or released eastward along the Cuban coast, can influence the basin-wide LC/FC evolution.

Known processes on LC/FC evolution include the impact of flow conditions at the Yucatan entrance, which may affect the shedding of anticyclonic rings from an extended LC in the GoM (Candela et al., 2002; Oey,

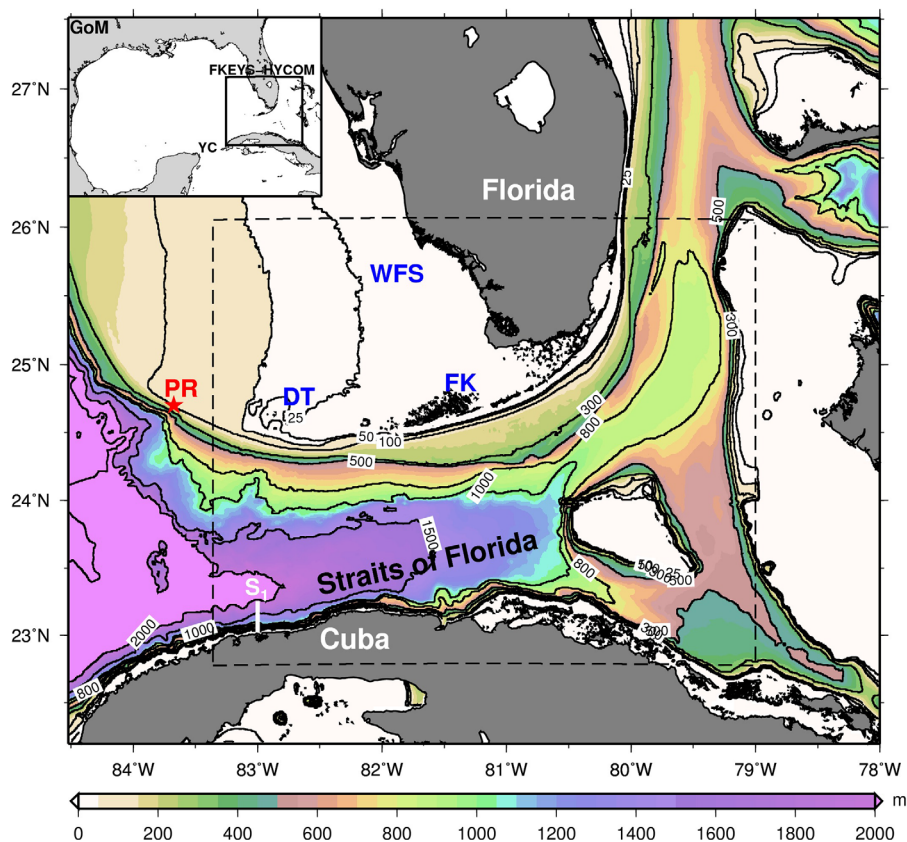


**Figure 1.** Bathymetry (m) of the FKEYS-HYCOM domain; certain isobaths are marked. Geographical locations mentioned in the text: GoM, Gulf of Mexico; YC, Yucatan Channel; Florida, Cuba, Straits of Florida; WFS, West Florida Shelf; DT, Dry Tortugas; FK, Florida Keys. The buoy station at the Pulley Ridge (PR) reef is marked with a red star. The smaller model domain of the 2004–2012 simulations is indicated with a black dashed box and section  $S_1$  is marked with a solid white line (83°W, 23°N–23.25°N).

2004). These so-called LC Eddies (LCEs) undergo a series of detachments and reattachments that may lead to eventual full separation from the main LC body (Hurlburt & Thompson, 1980; Sturges et al., 1993; see also review in Oey et al., 2005) and cause the LC to dramatically change from a northward expansion (extended LC approaching the northern GoM) to a retracted position (“young” LC approaching Cuba). The young LC phase and the rapid anticyclonic turn of the Yucatan flow into the Straits of Florida have been associated with strong eastward flow over the Dry Tortugas and lower Florida Keys (Lee et al., 1995; based on moored and satellite observations). Although the formation, detachment, and full separation of the LCE (followed by westward advection) have been studied extensively, the anticyclonic flow characterizing the southward retracted, young LC has only been considered as related to the eventual northward growth to a newly extended LC phase. Similarly, although FC meandering has been studied as related to large-scale forcing (Johns & Schott, 1987; Schott et al., 1988) and mesoscale cyclonic eddies traveling along the Florida Keys (north of the FC front; Fratantoni et al., 1998; Kourafalou & Kang, 2012; Lee et al., 1995), the contribution of eddies south of the FC front (along northern Cuba) has not been considered, even though they might be of potentially equivalent impact on the circulation and the biophysical transport processes in the Straits of Florida. Moreover, the role of mesoscale cyclonic eddies traveling around the LC/FC system on the LCE detachment have been highlighted in several studies (e.g. Androulidakis et al., 2014; Chérubin et al., 2005, 2006; Le Hénaff et al., 2012a; Le Hénaff et al., 2014; Schmitz, 2005; Von Arx et al., 1955; Zavala-Hidalgo et al., 2003). These studies mainly focused on understanding the LC/FC evolution and the LCE shedding process, but did not study the downstream current dynamics, which include the evolution of the CubAN eddies. We note that we consider mesoscale eddies in the Straits of Florida those at the range of 30–100 km diameter, based on a baroclinic Rossby radius of deformation at  $\sim 30$  km in this region (Kourafalou & Kang, 2012; Shay et al., 2007) and the maximum diameter reported from both model and observations (Lee, 1975; Sponaugle

et al., 2005). The part of the Straits of Florida relevant to the present study is the southern one (West to East orientation), before the Straits curve northward, after the Florida Keys chain (Figure 1).

The FC variability and the associated frontal eddies along its northern front affect the coastal areas around South Florida (Kourafalou & Kang, 2012). The FC is either in a northern position (approaching southern Florida and the Florida Keys) or deviates southward, toward Cuba. This type of modulation influences both the local dynamics and the broader oceanic current variability, since the FC is part of the large-scale Gulf Stream system. Herein, we investigate the interaction between the FC meandering and frontal anticyclonic eddies, evolving over its southern front along the Cuban coast. The description and analysis of the synergy between FC meandering, cyclonic frontal eddies at its north and anticyclonic CubAN eddies at its south are expected to improve the understanding of connectivity pathways between the Caribbean Sea and the Atlantic Ocean and thus aid the management of regional important coastal and reef ecosystems.

Our study is motivated by the need to better understand the mechanisms controlling the LC/FC variability, with broader implications on the dynamics of the interior GoM basin and the Straits of Florida, as well as slope exchanges with the shelf areas of the region. The main scope of the paper is to investigate the dynamics of CubAN eddies, which we define as anticyclones that are formed and evolve south of the FC (between the FC and Cuba) and within the outflow of warm Caribbean waters through the Yucatan Channel and around the northwestern tip of Cuba. More precisely, our goals are to define and identify CubAN eddies, to quantify their presence, to characterize the conditions in which they occur, and to describe their interaction with the LC/FC system, based on a few study cases. In addition, we examine upwelling filaments and cyclonic eddies along the Cuban coast and identify their role in the evolution of the CubANs. The study covers a protracted period of 13 years (2004–2016), employing high-resolution model simulations (section 2.1) and observations (drifters, satellite, and buoy data, section 2.2) to accomplish the study's goals.

## 1.2. Description of Cuban Anticyclonic Eddies (CubANs)

Similarly to the cyclonic, cold-core eddies that travel along the LC/FC oceanic current system, distinctive anticyclonic cores are identified within the LC core and south of the FC, along the northern Cuban coast. Oey et al. (2003), based on numerical experiments, showed that when Caribbean anticyclonic eddies complete their northward passage through the Yucatan Channel, part of their mass may transport along the Straits of Florida. However, they did not study the formation and evolution of the separate anticyclones we have identified downstream of Yucatan, and their interactions with the large-scale GoM circulation; these topics remain poorly understood.

To aid the description of study processes, we will distinguish two types of CubAN eddies: type "A" is present when there is a closed anticyclonic cell within the LC core over northwestern Cuba during the LCE shedding process that leads to a retracted LC; type "B" are individual, distinct anticyclonic eddies that have been separated from the main LC core and have advanced eastward, along the northern Cuban coast. Figure 2 presents four characteristic snapshots of LC evolution and the respective anticyclonic activity along the Cuban coast, based on satellite altimetry fields (see section 2.2 for data set information). Following Leben (2005), we define the LC front based on the 17 cm contour in Sea Surface Height (SSH) anomaly with respect to the basin mean SSH. We show a succession of GoM mesoscale variability in 2004, starting with a type "A" CubAN within the young LC (6 February), continuing with a type "B" that has moved eastward, away from the base of the extended LC (16 July), then an example of the extended LC phase when no CubANs are present (1 August) and finally coexisting type "A" and type "B" CubANs after the LC returned to a retracted position (5 September). We note that a type "A" CubAN is not identical to the young LC, as it is defined as a closed circulation anticyclonic cell within the base of the LC core. Both types can form during either fully retracted LC conditions or when the LC is still extended, but has acquired anticyclonic curvature due to the action of LC Frontal Eddies (LCFEs) acting to narrow the advancing LC neck. More than one type "B" can be shed from a young LC, leading to the possibility that a succession of type "A" and type "B" can be observed simultaneously. As the LC feeds into the FC at the western entrance of the Straits of Florida (at  $\sim 83^\circ\text{W}$ ), a strong southward curvature of the front can be seen. This curvature was previously attributed to the synergy of FC evolution with cyclonic eddies that move eastward from the Dry Tortugas along the Florida Keys, north of the FC front (Kourafalou & Kang, 2012). We will show that the FC undulations within the Straits of Florida are also related to the evolution of anticyclonic CubANs south of the FC.

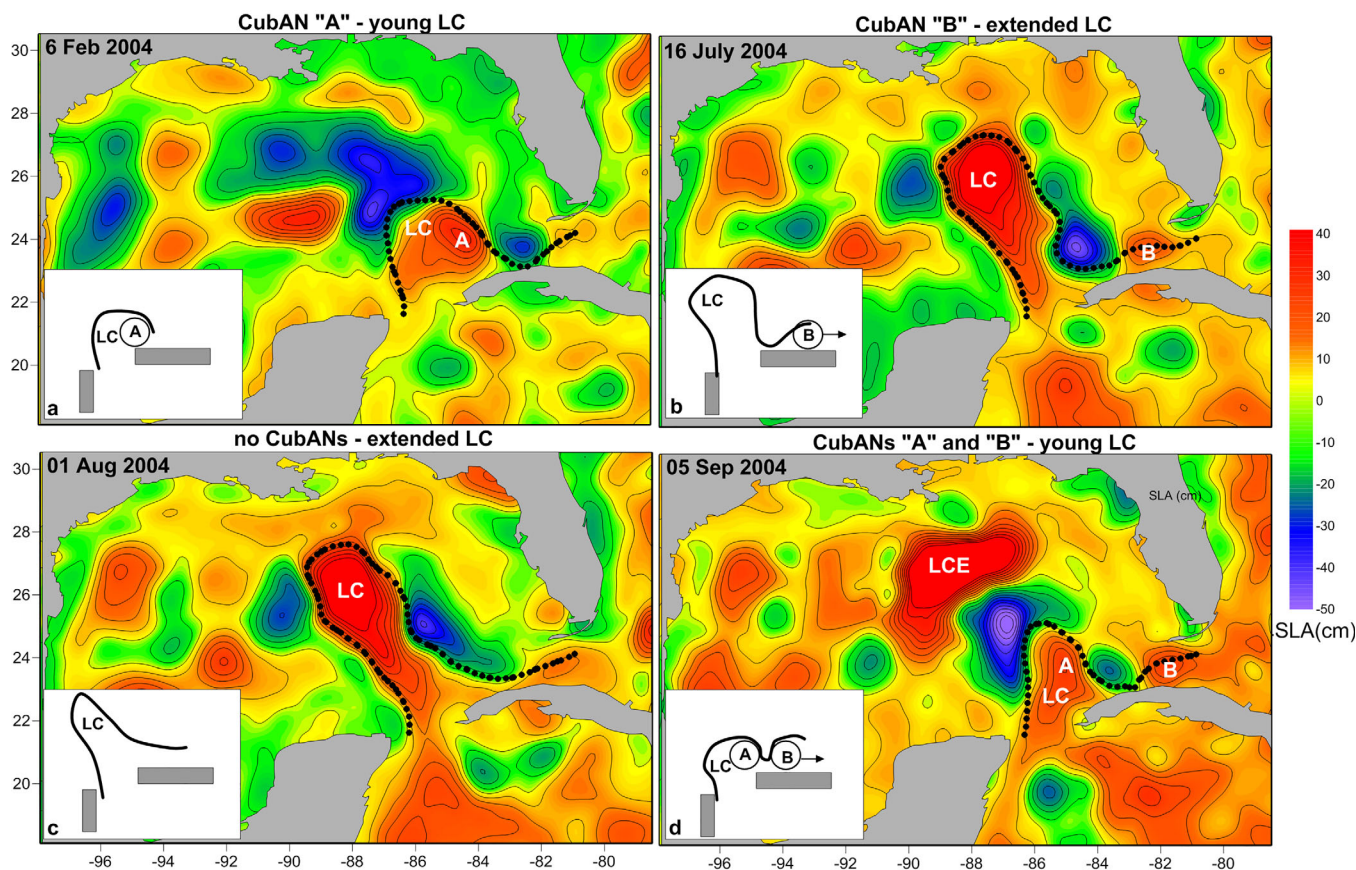


**Figure 2.** Maps of AVISO Sea Level Anomaly (SLA, cm) and the respective schematic of mesoscale features: Loop Current (LC), Cuba Anticyclones (CubANs) type “A” and type “B” on (a) 6 February 2004, (b) 16 July 2004, (c) 1 August 2004, and (d) 5 September 2004.

## 2. Methods and Data

### 2.1. Model Description

The hydrodynamic simulations are based on the Florida Straits, South Florida, and Florida Keys Hybrid Coordinate Ocean Model (FKEYS-HYCOM; Kourafalou & Kang, 2012) and cover a 13 year period (2004–2016). HYCOM (<http://hycom.org>; Bleck, 2002; Chassignet et al., 2003; Halliwell, 2004) is a state-of-the-art, three-dimensional hydrodynamic model with advanced mixing schemes and employs a flexible (hybrid) vertical coordinate system (isopycnal, Cartesian, and sigma discretizations) that is advantageous for the topographically complex study area (Figure 1).

The community available HYCOM code can be run with or without data assimilation. FKEYS-HYCOM is free running (no data assimilation) and nested in a coarser application of HYCOM for the GoM (GoM-HYCOM; Gierach et al., 2009; Kourafalou et al., 2009; Le Hénaff et al., 2012b; Mariano et al., 2011; Mezić et al., 2010; Paris et al., 2012; Prasad & Hogan, 2007; Valentine et al., 2012) which employs the Navy Coupled Ocean Data Assimilation (NCODA; Cummings, 2005), an oceanographic version of the MVOI (MultiVariate Optimum Interpolation) technique widely used in operational atmospheric forecasting systems (Daley, 1991). The ocean analysis variables in NCODA are temperature, salinity, geopotential (dynamic height), and velocity. The FKEYS-HYCOM (which has been running from 2004 to date) thus receives realistic boundary forcing, which is updated daily. Nested models (even when free running) are capable to add value on data-assimilative, outer models, as they are generally of higher resolution, employ better coastal topography, may have more details in coastal physics and are often forced with higher-resolution/higher-frequency fields (see review and examples in Kourafalou et al., 2015a, 2015b).

FKEYS-HYCOM employs 26 hybrid vertical layers and significantly high horizontal resolution of  $1/100^\circ$ , or  $\sim 900$  m (as compared to  $1/25^\circ$ ,  $\sim 3.6$  km in the GoM-HYCOM outer model). The model domain for the

2004–2012 period covers the area from 79.0°W to 83.4°W and from 22.8°N to 26.1°N (dashed box in Figure 1). The model domain was then extended (2013 to date), covering a larger area from 78.0°W to 84.52°W and 22.18°N to 27.5°N (Figure 1) with the same vertical discretization. The 2004–2012 period topography was derived from the 2 min NRL DBDB2 global data set with a minimum depth of 2 m and with corrected Keys passages through local data (Kourafalou & Kang, 2012). The upgraded topography for the extended domain was derived from a high-resolution (1/100°) regional GoM bathymetry developed at the Florida State University/COAPS with a minimum depth of 1 m. The FKEYS-HYCOM vertical coordinates are maintained in isopycnic mode in the “open sea” domain (e.g., Straits of Florida), they smoothly transform to bottom following (sigma) and/or Cartesian (fixed z level) coordinates in the mixed layer, and in the coastal and shelf areas (e.g., Florida Shelf, northern Cuban coast and shallow banks). Atmospheric forcing is provided by two different 3-hourly products from the U.S. Navy: (1) The Coupled Ocean/Atmospheric Mesoscale Prediction System (COAMPS, Hodur, 1997; Hodur et al., 2002) until 2013 and (2) the Navy Global Environmental Model (NAVGEM, Metzger et al., 2013) from 2014 and later. The former has a spatial resolution of approximately 27 km while the latter has spatial resolutions of 0.5° till 2015 and 0.28° for 2016. The FKEYS-HYCOM has been validated with satellite (Kourafalou & Kang, 2012) and in situ (Kourafalou et al., 2015a) data, showing additional skill in capturing eddy evolution in the Straits of Florida, as compared to the coarser GoM-HYCOM model. In tandem with physical and biological data, this high-resolution, free-running, nested model has been used in previous studies to investigate the biophysical larval transport along the Keys (Sponaugle et al., 2012), to capture the spatial-temporal scales of circulation influencing larval dispersal in the region between Pulley Ridge coral reef and Florida Keys (Vaz et al., 2016), to simulate the mesoscale cyclonic eddies on FC meandering (Kourafalou & Kang, 2012), and to provide high-resolution 7 day forecasts of sea-state around South Florida and within the Straits of Florida (<http://coastalmodeling.rsmas.miami.edu/>).

## 2.2. Observations

Three satellite data sets are incorporated in the study. The first data set is from the Group for High Resolution Sea Surface Temperature (GHRSSST; <https://www.ghrsst.org/>), which includes gridded Sea Surface Temperature (SST) fields. We use the GHRSSST Level 4 SST fields (produced by GHRSSST daily Level 2 data; Donlon et al., 2009), covering the Straits of Florida region (Figure 3a) with horizontal resolution of 1–2 km. These SST fields are employed to evaluate the model performance over the CubANs propagation area (section 3.1) and to investigate the inter-annual variability and SST trend during the entire study period (section 3.2). The GHRSSST data are also used to detect warm and cold eddy formation and to investigate upwelling processes along the northern Cuban coast. The second satellite data set is the Archiving, Validation and Interpretation of Satellite Oceanographic Data (AVISO; <http://www.aviso.altimetry.fr>) that includes the Sea Level Anomaly (SLA) estimated with altimeters in orbit and the Mean Dynamic Topography (MDT). When combined, SLA and MDT represent the Maps of Absolute Dynamic Topography (MADT), which is comparable to the model SSH. The MADT data have 0.25° resolution and are used to investigate both the LC evolution, based on the 17 cm SSH anomaly contour (Leben, 2005), and the formation of cyclonic and anticyclonic eddies over the study region and the broader GoM. The eddy horizontal structure and the upwelling events can be also identified in ocean color maps derived from MODIS/Aqua chl *a* (<http://optics.marine.usf.edu>), consisting the third satellite data set used in this study. As the model is free running (no data assimilation), all the model-observation comparisons are considered as independent evaluations.

In addition to satellite data, we use in situ drifter data from the Global Drifter Program (GDP). This program has followed the Surface Velocity Program (SVP) started in 1979 to provide measurements of near-surface ocean currents worldwide at 15 m depth (Niiler & Paduan, 1995; Reverdin et al., 2003). SVP drifters are composed of a spherical buoy at the surface, connected to a nylon holey sock drogue (sea anchor) so that the drifting system tracks the water displacement at 15 m (Lumpkin & Pazos, 2007). The global SVP drifter array is managed by the National Oceanic and Atmospheric Administration's Atlantic Oceanographic and Meteorological Laboratory (NOAA/AOML), with the objective of maintaining global 5° by 5° world ocean coverage, corresponding to approximately 1,250 drifters simultaneously at sea. The GDP data include drifter positions and dates interpolated to regular 6 h intervals, along with the associated velocity vectors estimated as 12 h centered differences, and the measured SST. We use two drifter trajectories, from GDP drifters #70325 and #145522. An additional in situ data set, used to evaluate the model results, was derived by the Acoustic

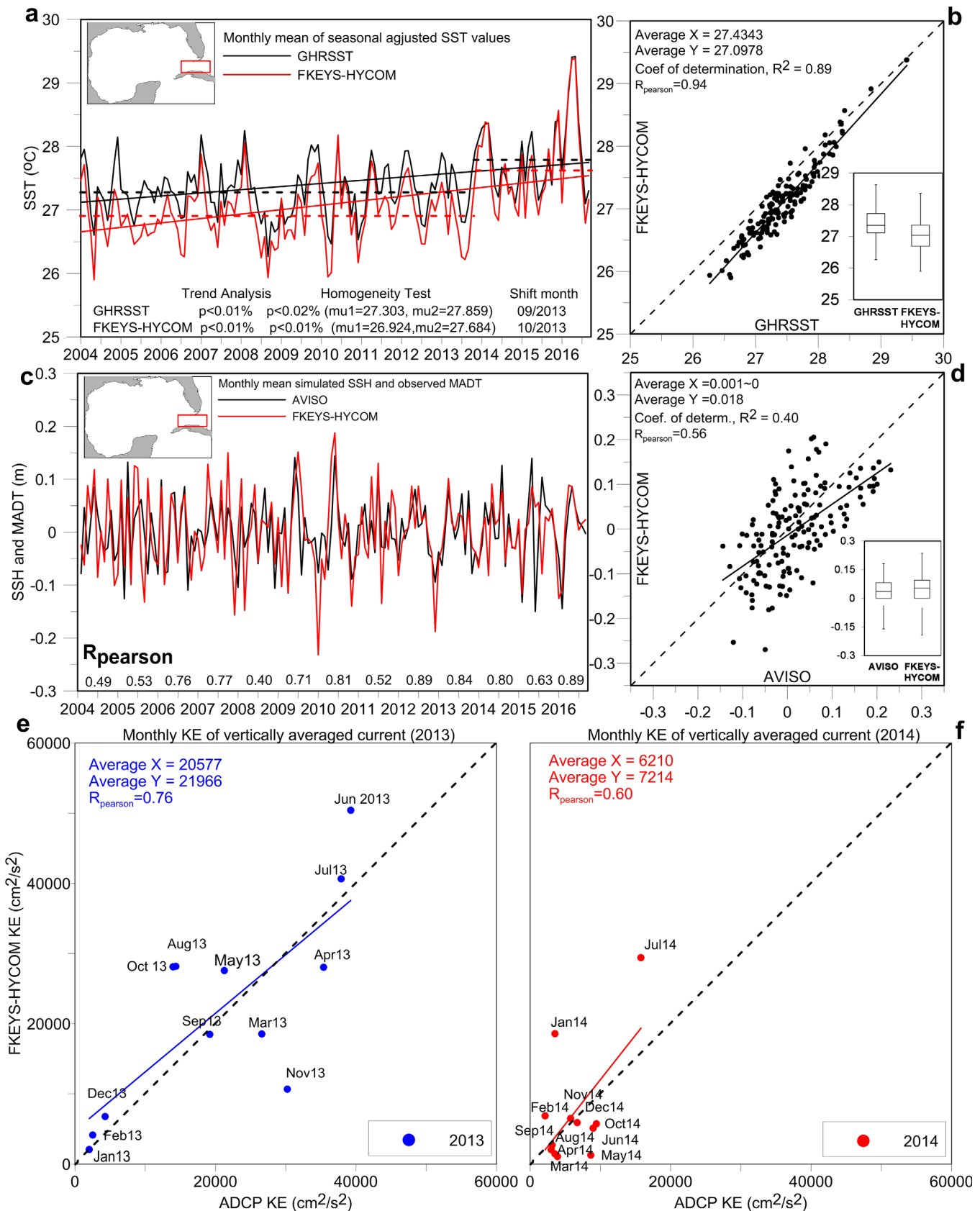


Figure 3. (continued)

Doppler Current Profiler (ADCP) at the Pulley Ridge buoy (Figure 1), covering the years 2013 and 2014. These observations are used to evaluate the vertically averaged simulated currents (Figure 3) over a region of the Straits of Florida, which is strongly affected by the LC/FC system.

### 3. Results

#### 3.1. Evaluation of the Model Simulation

We employ the 2004–2016 FKEYS-HYCOM simulation that provides three-dimensional 6-hourly fields of temperature, salinity, SSH, and currents. Model evaluation against satellite and in situ data has been included in previous studies (section 2.1), showing the good performance of the model in describing the coastal and shelf physical characteristics and the broader dynamics in the Straits of Florida. Here we provide additional inter-annual comparisons with satellite observations during the 13 year study period.

The formation and especially the propagation of anticyclonic CubANs take place along the northwestern Cuban coast and in the Straits of Florida (Figure 2). We examine the SST over an area that includes the southern Straits of Florida (Figure 3a), which encompasses the main region of CubANs evolution. The seasonally adjusted values (seasonality removed) are strongly related to the FC evolution and the associated frontal cyclonic (cold-core) and anticyclonic (warm-core) eddies. The mean monthly seasonally adjusted time series over this specific area during 2004–2016, derived from FKEYS-HYCOM and GHRSSST data, are presented in Figure 3a. The average value of the simulated and observed time series is  $\sim 27.1^\circ\text{C}$  and  $27.4^\circ\text{C}$ , respectively. The linear fit of the two series (Figure 3b) is very close to the  $x = y$  identity line with stronger agreement over higher levels ( $>28^\circ\text{C}$ ), which are more related to the anticyclonic activity and the FC pattern; very high coefficient of determination ( $R^2 = 0.89$ ) and Pearson correlation ( $R_{\text{pearson}} = 0.94$ ) were computed. The box plots, derived for the entire study period, are similar for both cases; the upper (lower) quartile is  $27.7$  ( $27.1$ ) $^\circ\text{C}$  for GHRSSST and  $27.3$  ( $26.7$ ) $^\circ\text{C}$  for FKEYS-HYCOM, showing same respective distances from the maximum (minimum) values. Moreover, the variability outside the upper and lower quartiles is similar in both time series. The interquartile range is  $0.60$  for data and  $0.66$  for model.

The inter-annual SST evolution shows a clear increasing trend in both the simulated and observed values. This trend is statistically significant since both simulated and observed  $p$  values (Mann Kendall (MK) test; Kendall, 1975; Mann, 1945) are significantly low ( $<0.01\%$ ). If the  $p$  value, computed by the MK test, is less than the considered significance level (e.g., 5%), the hypothesis that there is no trend is rejected. Rejecting this hypothesis indicates that there is a trend in both time series, while accepting the hypothesis ( $p$  values  $> 5\%$ ) indicates that no significant trend is detected. The model also succeeded to efficiently simulate the high (e.g., 2016: SST  $> 29^\circ\text{C}$ ) and low (e.g., 2008: SST  $< 26.5$ ) peaks, revealing similar inter-annual variability between the two series. The homogeneity test of the two variations shows that there is a date at which there is a change in the data (both series show homogeneity  $p$  values smaller than 5%;  $p_{\text{GHRSSST}} < 0.02\%$  and  $p_{\text{FKEYS-HYCOM}} < 0.01\%$ ). Homogeneity tests help determine if series can be considered as homogeneous over time ( $p > 5\%$ ), or if there is a time at which a significant change occurs ( $p < 5\%$ ). In both cases, the date when a notable shift occurred was in fall 2013 (September for GHRSSST and October for FKEYS-HYCOM). The averaged values before ( $\mu_1$ ) and after ( $\mu_2$ ) the shift are similar between the two time series (Figure 3a). The shift ( $\mu_2 - \mu_1$ ) is greater than half degree and ranges around  $0.55^\circ\text{C}$  and  $0.76^\circ\text{C}$  for observed and simulated time series, respectively. In section 3.2, we show that there is a possible connection between the shift that occurred after 2013 and the presence of CubANs over the study region.

**Figure 3.** Temporal evolution of (a) seasonally adjusted monthly Sea Surface Temperature (SST), as derived from GHRSSST (black line) and FKEYS-HYCOM (red line) and (c) monthly detrended Maps of Absolute Dynamic Topography (MADT) and Sea Surface Height (SSH), as derived from AVISO (black line) and FKEYS-HYCOM (red line), respectively, averaged over the Straits of Florida domain (red box in map insert) during the 2004–2016 period. The linear trends and the  $p$  values for both the trend test (solid lines) and homogeneity test (dashed lines) and annual Pearson correlation coefficients ( $R_{\text{pearson}}$ ) are also shown. Scatter diagram, linear fit, and box plots of observed and simulated monthly mean of (b) seasonally adjusted SST values and (d) SSH-MADT values. The mean values, the coefficients of determination ( $R^2$ ), and Pearson correlation ( $R_{\text{pearson}}$ ) are also shown. Comparison of monthly Kinetic Energy (KE) of vertically averaged currents between the FKEYS-HYCOM simulation and the respective measured currents (ADCP) at Pulley Ridge (Figure 1) for (e) 2013 (blue) and (f) 2014 (red). The linear fit (solid lines), the Pearson correlation ( $R_{\text{pearson}}$ ), and the mean values of each year are also presented with the respective colors.

The mean monthly detrended evolution of MADT over the Straits of Florida (derived from the AVISO fields, see section 2.2) is presented in Figure 3c. Because the CubANs have a rather small diameter (<100 km) and are close to the Cuban coasts, mapped altimetry products have a limited ability to precisely represent them. Indeed, altimetry measurements suffer from the proximity of the coast, in a distance up to 50 km (Roblou et al., 2011). In addition, the mapped products have difficulties resolving features of dimension smaller than  $\sim 100$  km characteristic length, determined from the along-track data separation (Dussurget et al., 2011). This is why it is not possible to make a census of the CubANs based on altimetry only, because altimetry maps might miss small CubAN eddies, and misplace the center and boundaries of others. However, mapped altimetry products are able to characterize larger-scale circulation patterns, such as the extension of the Loop Current and its (large) meanders, which are closely linked to eddy activity. This is why we present here a comparison between the observed MADT and the model SSH, averaged over the Straits of Florida. Overall, the respective simulated SSH evolution during the entire study period agrees with the observed MADT, showing positive and high Pearson correlation coefficients ( $R_{pearson}$ ) in most of the years. Almost all coefficients are higher than 0.5 and in many cases range in very high levels close to 0.90 (e.g., 2012). Although the comparison is not as good as in the case of the GHRSSST observations, which might be attributed to the low resolution of the AVISO fields, the general agreement between the two time series supports the ability of the model to efficiently describe both the FC evolution and the associated mesoscale dynamics in the Straits of Florida, in agreement with Kourafalou and Kang (2012). Peaks (positive SSH) and lows (negative SSH) correspond to strong FC (and/or anticyclonic circulation) and weak FC (and/or cyclonic circulation), respectively. The observed-simulated pairs are aligned along the  $x = y$  identity line (Figure 3d) with lower alignment than in the case of the SST comparison, but still positive coefficient of determination ( $R^2 = 0.40$ ). The Pearson correlation ( $R_{pearson} = 0.56$ ) is less than the respective coefficient of the SST comparison, but it is positive and more than 50%, indicating the good performance of the model to represent the SSH interannual variability in the Straits. Box plots confirm that in both cases the medium SSH values are very close. The model values are generally more spread out, but with similar spreading to the data for the higher values, which are more related to anticyclonic activity and the occurrence of CubANs.

Additional comparisons of model fields with current measurements employ the Kinetic Energy (KE) for years 2013 (Figure 3e) and 2014 (Figure 3f) at the location of the Pulley Ridge reef ADCP mooring (marked on Figure 1), which is greatly influenced by the LC variability (Vaz et al., 2016). Very high KE levels were both simulated (mean KE = 21,966  $\text{cm}^2/\text{s}^2$ ) and observed (mean KE = 20,577  $\text{cm}^2/\text{s}^2$ ) for 2013. On the contrary, both model and data yielded low mean monthly KE values for most of 2014 (mean KE < 7,500  $\text{cm}^2/\text{s}^2$ ). In both years, the correlation coefficients ( $r_c$ ) are high, while the linear fits are very close to the  $x = y$  identity line. These results show that the FKEYS-HYCOM can adequately simulate the local circulation near the western entrance of the Straits of Florida (where the CubAN eddies develop and evolve), while correctly incorporating the regional circulation patterns (LC/FC evolution) through its nesting within the coarser, data assimilative GoM-HYCOM model (section 2.1).

### 3.2. Inter-Annual Variability of CubANs Related to LC/FC Evolution

Based on the definition of the CubAN anticyclonic eddies introduced in section 1.2, the periods of CubANs presence have been identified for the years 2004–2016. The identification of a CubAN is mainly based on the simulated SSH fields, supported by the respective satellite altimetry maps, providing the high positive SSH values over the northwestern Cuban coast that reflect the anticyclonic circulation. The simulated surface currents were employed to identify the anticyclonic circulation of these mesoscale eddies. An additional confirmation of the CubAN evolution is based on satellite and modeled high SST cores (warm anticyclonic eddies), while the available ocean color maps also provided information about the shape and extension of CubANs. All type “A” and type “B” CubANs (Figure 2) over the 13 year study period were identified and grouped in continuous periods of detection along the Straits of Florida. The longest periods of CubANs appearance (over 150 days) occurred on 2009, 2012, 2013, and 2016 (Figure 4). The mean annual frequency, averaged for the entire 13 year period is 34.2%. This means that CubANs are present over the study region during more than 1/3 of the time. The highest rate was computed for summer periods, as 37.3% of all CubANs (CubAN presence in Seasonal days divided by CubAN days) occurred during that season.

We also estimated the position of FC and LC fronts, to examine possible connection with the evolution of CubANs. The FC position was estimated based on the latitude of the 20°C isotherm at 150 m along the

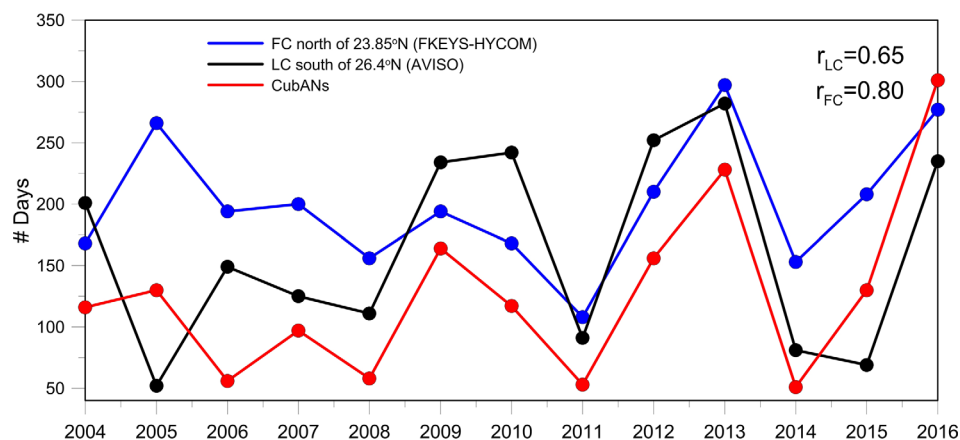


**Figure 4.** Time series of the annual number of days when the Florida Current (FC) position (latitude of the 20°C isotherm at 150 m along 83°W) is located north of 23.85°N (blue line), and when the Loop Current (LC) position (northernmost latitude of the 17 cm contour in Sea Surface Height anomaly with respect to basin mean) is located south of 26.4°N (black line) for the 2004–2016 period, as derived from the FKEYS-HYCOM and AVISO data, respectively. The corresponding number of days of CubAN presence for each year is indicated with a red line. The 23.85°N and 26.4°N latitudes are the average zonal positions of the FC and LC, respectively, during the 2004–2016 period. The correlation coefficients between the LC and CubANs time series ( $r_{LC}$ ) and the FC and CubANs time series ( $r_{FC}$ ) are also given.

83°W meridional (Kourafalou & Kang, 2012), as derived from the FKEYS-HYCOM simulation. The northern extension of the LC front was computed based on the 17 cm SSH anomaly contour derived from the AVISO data (section 2.2). The temporal evolution of the northern LC front actually represents the changes in LC extension, including its growth toward the northern GoM, the LCE detachment and shedding periods and the formation of the young LC over the western entrance of the Straits of Florida.

We found that periods with presence of CubANs are aligned with periods when: (a) the FC shifts northward at the western entrance of the Straits of Florida and (b) the LC starts to get “necked down” (narrowing of the distance between the LC western and eastern sides) under the influence of cyclonic LCFEs, which have been found to play an important role in the processes that lead to LCE separation (Le Hénaff et al., 2012a). The former can have a profound influence on the FC meandering within the Straits. Kourafalou and Kang (2012) connected this meandering with the evolution of cyclonic eddies to the north of the FC front, along South Florida and the Florida Keys. The cyclones were considered to either evolve from LCFEs traveling southward along the eastern side of the LC or be formed locally, when the FC was in a northward position near the Straits entrance. We now show that CubANs play a profound role in these processes, as they evolve to the south of the FC front, along the northern Cuban coast.

Figure 4 presents the time series of yearly estimate of the number of days in which: (1) the FC is displaced northward in the Straits of Florida (north of 23.85°N, its average position during our study period); (2) the LC is retracted in the GoM (south of its average 26.4°N value); and (3) the number of days of CubAN presence along the Cuban coast. The correlation coefficient between the occurrence of northern FC and the presence of CubANs is high and positive ( $r_{FC} = 0.80$ ), supporting the strong relationship between both patterns. Similarly, the presence of CubANs is strongly related to the LC necking down phase that eventually leads to LCE shedding and the formation of a young LC over the northwestern region of Cuba ( $r_{LC} = 0.65$ ). The variations in annual occurrence frequencies of northern FC, retracted LC, and CubAN presence are very similar along the entire study period. All years show periods of CubAN presence that starts from ~50 days (e.g., 2006, 2008, 2011, and 2014) and reaches as high as ~300 days. The highest numbers were calculated for 2013 and 2016 (around 220 days in 2013 and almost 300 days in 2016) with 210 (2013) and 260 (2016) days of continuous CubAN activity during summer and autumn (not shown). These peaks were related to the LC and FC showing the longest periods of southern and northern positions, respectively. This finding agrees with the SST increase that was computed by the homogeneity test of the GHRSSST data set (Figure 3a), which supports the large number of warm anticyclonic activity during 2013 and a respective high peak in 2016. These long periods of CubAN presence contributed to the higher SST values, derived from the homogeneity test for the 2013–2016 period ( $\mu_2 = 27.859^\circ\text{C}$  for GHRSSST and  $\mu_2 = 27.684^\circ\text{C}$  for FKEYS-HYCOM;

Figure 3a), in comparison with the 2004–2012 period ( $\mu_1 = 27.303^\circ\text{C}$  for GHRSSST and  $\mu_1 = 26.924^\circ\text{C}$  for FKEYS-HYCOM; Figure 3a). We deduce that the observed and modeled 2013–2016 shift to higher temperatures was influenced by the sustained periods of occurrence peaks for warm-core CubAN eddies in late 2013, early 2014, early and late 2015, and during the entire 2016. The overall increasing trend in the number of CubANs (Figure 4) agrees with the increasing SST in the Straits of Florida over the study period (Figure 3). In order to estimate the significance of the relationship between the three time series, we also computed the  $p$ -values for significance level 95%, which indicates how unlikely a given correlation coefficient  $r$  will occur given no relationship in the population. In both cases (LC-CubANs and FC-CubANs), the  $p$ -values are significantly smaller than 5% ( $p\text{-value} < 0.001$  for  $r_{FC}$  and  $p\text{-value} = 0.019$  for  $r_{LC}$ ), indicating that the correlations between the occurrence frequencies are statistically significant.

There are also a few periods (in 2004, 2005, 2006, and 2011), when, although the LC was extended, several CubANs were formed and the FC shifted to the North. Therefore, the anticorrelation between the FC and LC position temporal evolution is weaker for those periods, revealing even positive Pearson coefficients (e.g.,  $r = 0.17$  for 2006). Moreover, the small number of days of retracted LC in 2005 (Figure 4), which indicates a predominantly northward LC, was not associated with a reduction of CubAN presence; the number of days of CubAN presence ( $\sim 125$ ) and of northward FC shift ( $\sim 270$ ) were both high. On the contrary, the increase in the number of days with a retracted LC in 2006 ( $\sim 150$ ) was not associated with a respective increase in the number of days of northward FC displacement and of CubAN presence; the LC remained south of  $26.4^\circ\text{N}$  but north of  $25.5^\circ\text{N}$  in autumn and winter of 2006, without contributing to the formation of CubANs. These exceptions are related to the general circulation of the region, in particular the cyclonic activity (see section 4.1). The high occurrence frequency of the LC over the western Straits of Florida in 2013 (more than 250 days) is also supported from both modeled and observed currents at the Southwestern Florida Shelf (Figures 3e and 3f), whose local circulation is strongly affected by the vicinity of the LC; LC shifting toward the shelf usually coincides with its young phase (south of  $26.4^\circ\text{N}$ ), increasing the southwest currents at the Pulley Ridge buoy.

#### 4. Discussion

Five characteristic periods (five cases; Table 1) of CubAN evolution are discussed hereafter, in order to describe: their interaction with the LC/FC system (Case #1, Case #2, and Case #3; section 4.1), the eddy characteristics and structure of a CubAN along the Cuban coast (Case #3, Case #4, and Case #5; section 4.2), the related transport processes (all cases; section 4.3), and the CubANs interaction with local dynamics (Case #2 and Case #5; section 4.4). Our discussion distinguishes between the fully extended LC (no LCE) and the young LC phase, which we define from the onset of LCE detachment to the full LCE separation and retracted LC. We employ near-surface currents and SSH fields from the FKEYS-HYCOM simulation, in tandem with MADT maps derived from AVISO data for the same dates. As noted in section 3.1, the shape of CubAN eddies that are in the lower part of the mesoscale range (30–100 km diameter) might not be well represented in AVISO maps, due to the current resolution limitation of altimetry and their proximity to the Cuban coast. Therefore, CubANs might be under-represented or even missed on these maps, if their size is particularly small, or if they are located between two satellite tracks. However, the use of AVISO fields does distinguish the general anticyclonic and cyclonic mesoscale circulation patterns within the Straits of Florida.

**Table 1**  
*Period, Loop Current (LC) Extension Phase, Florida Current (FC) Position, Cyclonic Activity, CubAN Name, and Type ("A" and/or "B") of the Five Study Cases of CubAN Evolution*

	Period	LC	FC	CubAN activity	Cyclonic activity and upwelling
Case #1	Apr. 2004	Extended	$\sim 24.25^\circ\text{N}$	CA1 ("B")	C1, C2
Case #2	Jun. 2004	Young	$\sim 24.3^\circ\text{N}$	CA2 ("A"), CA3 ("B"), CA4 ("B")	C2, C3, upwelling
Case #3	Oct. 2007	Young	$\sim 24.35^\circ\text{N}$	CA5 ("A")	C4, C5
Case #4	Oct. 2012	Young	$\sim 24^\circ\text{N}$	CA6 ("A," "B"), CA7 ("A")	C6
Case #5	Aug. to Sep. 2016	Young	$\sim 24.2^\circ\text{N}$	CA8 ("A," "B"), CA9 ("B")	C7, C8, upwelling

#### 4.1. CubAN Formation and LC/FC Dynamics

Case #1 (Figures 5a and 5b) is at the beginning of April 2004, when the LC extension over the eastern GoM almost reached 27°N, while several cyclonic eddies occurred along its front. Satellite altimetry confirms that the LC was extended toward the northern GoM, while no LCE detachments were observed. Two cyclonic LCFEs were detected along the LC eastern front: C1 over the entrance of the Straits of Florida and C2 along the slope of the West Florida Shelf. The model simulation shows eastward currents up to 1 m/s and no anti-cyclonic activity inside the Straits during that period. The estimated position of the FC front on 1 April is very south, around 23.45°N, very close to the Cuban coast (Figure 5a). The cyclonic LCFEs evolving along the LC during April moved southward, with C2 participating in the separation of an anticyclonic eddy from the bottom of the LC core over the northwestern tip of Cuba at the end of April (Figure 5b). Although the LC was still well extended over the eastern Gulf (~27°N), a type "B" CubAN was shed and began to propagate toward the East (CA1). The C1 eastward advection and the C2 direct southward propagation over the eastern region contributed to the formation of this CubAN, which is both observed and simulated around 83°W. The increase in model SSH and satellite MADT and the anticyclonic circulation in the proximity of the Cuban coast are a clear indication of the CubAN formation, with significantly westward currents along the coast (~1 m/s), opposing the general eastward transport of the FC.

The second study case (Case #2, Figures 5c and 5d) is characteristic of CubAN formation during the process of LC necking down that can lead to a young LC. It is thus related to different LC characteristics from the previous case. After the end of Case #1, the cyclonic eddy C2 moved downstream (southward and then eastward) in the Straits of Florida, while another cyclonic LCFE (C3) participated in the onset of LCE detachment. Although the LC was extended and still attached to the LCE in the beginning of June, the C3 cyclone had almost necked down the LC, restraining its main body at the western entrance of the Straits of Florida. Two anticyclonic eddies, one type "A" over 83.5°W (CA2) and one type "B" over 81°W (CA3) formed along the Cuban coast during this young LC phase. We note that, although high sea elevation is shown in the data, CA3 does not appear clearly as an eddy cell on AVISO maps, which is presumably due to the gridded data limitation. During that period, C2 was located between the FC and the Florida Keys, participating in the meandering of the FC together with the CubANs propagation along the FC southern front. This case of FC/LC and CubAN synergy is the most common among the 2004–2016 events, when the majority of the anticyclonic activity along the Cuban coast is associated with the onset of the LCE formation and detachment, i.e., LC necking down conditions that eventually led to a young LC. In addition to the action of cyclonic eddies north of the FC (which are well known, see review in Kourafalou & Kang, 2012), smaller cyclonic eddy cells are detected to the south of the FC, along the Cuban coast that is under the influence of CubAN anticyclones. An example is shown in Figure 5c, where such an eddy is separating the CA2 and CA3 CubANs. These cyclonic cells are relatively short-lived and contribute to the separation of CubANs from the LC or from a prior type "A" CubAN, leading to type "B" formation. This is the case of CA3, which separated from CA2 and moved eastward, leaving the study area by mid-June (not shown). Similarly, type "B" CA4 separated from CA2 (Figure 5d, right) and evolved along the northern coast by 20 June, under the influence of upwelling filaments that contributed to its separation from CA2 and possibly supported the previous cyclonic cell (see also section 4.4).

Case #3 (Figure 6) took place in late 2007. The AVISO satellite fields present the LC northward extension in September 2007, when a mesoscale cyclonic eddy (C4) was present between the LC and the West Florida Shelf (Figure 6a). The SVP drifter #70325 (section 2.2) propagated along the western LC front and reached the northern tip of the LC around 27°N on 15 September 2007. No CubAN activity was detected during this period and the eastward FC moved in a southern orientation within the Straits of Florida. Then, C4 moved westward and started to create curvature at the east side of the LC front two weeks later (Figure 6b). This action triggered the formation of an anticyclonic eddy off northwestern Cuba, which had characteristics of a type "A" CubAN (CA5). This CubAN is also apparent in the simulated current and SSH fields over the same region (~83°W). The drifter had already propagated southward along the eastern LC front, reaching the base of the LC and getting trapped inside the CA5 CubAN. The FC started to move away from Cuba, toward the South Florida coast, due to the CA5 eddy presence in October 2007. The distinct structure of the CA5 CubAN is also confirmed by the second anticyclonic cycle of the drifter inside the vortex around 20 October (Figure 6c). The FC exhibited its most northern position of the year, very close to the southwest Florida shelf-break (~24.35°N). A second cyclonic LCFE (C5) at the west side of the LC combined action with C4 at

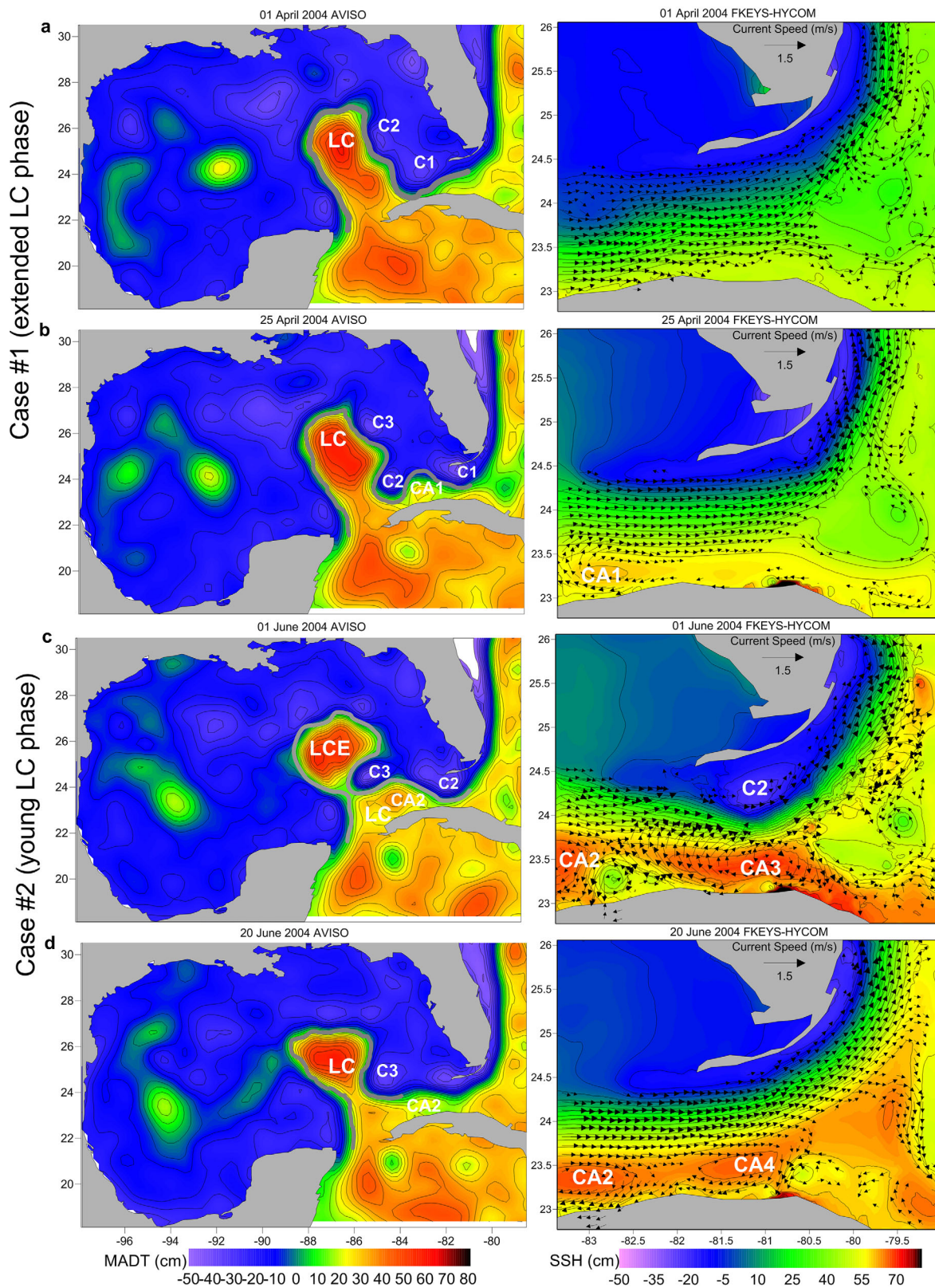


**Figure 5.** Cases #1 and #2 — Maps of (left) AVISO Mean Absolute Dynamic Topography (MADT) and (right) FKEYS-HYCOM Sea Surface Height (SSH) and current vectors (m/s) during (Case #1) extended Loop Current (LC): (a) 1 April 2004, (b) 25 April 2004 and during (Case #2) young LC phase (onset of LC Eddy, LCE, detachment): (c) 1 June 2004 and (d) 20 June 2004. The LC and LCE location (17 cm SSH contour, grey line), the major cyclones (C), and the CubANs (CA) are indicated on each map.

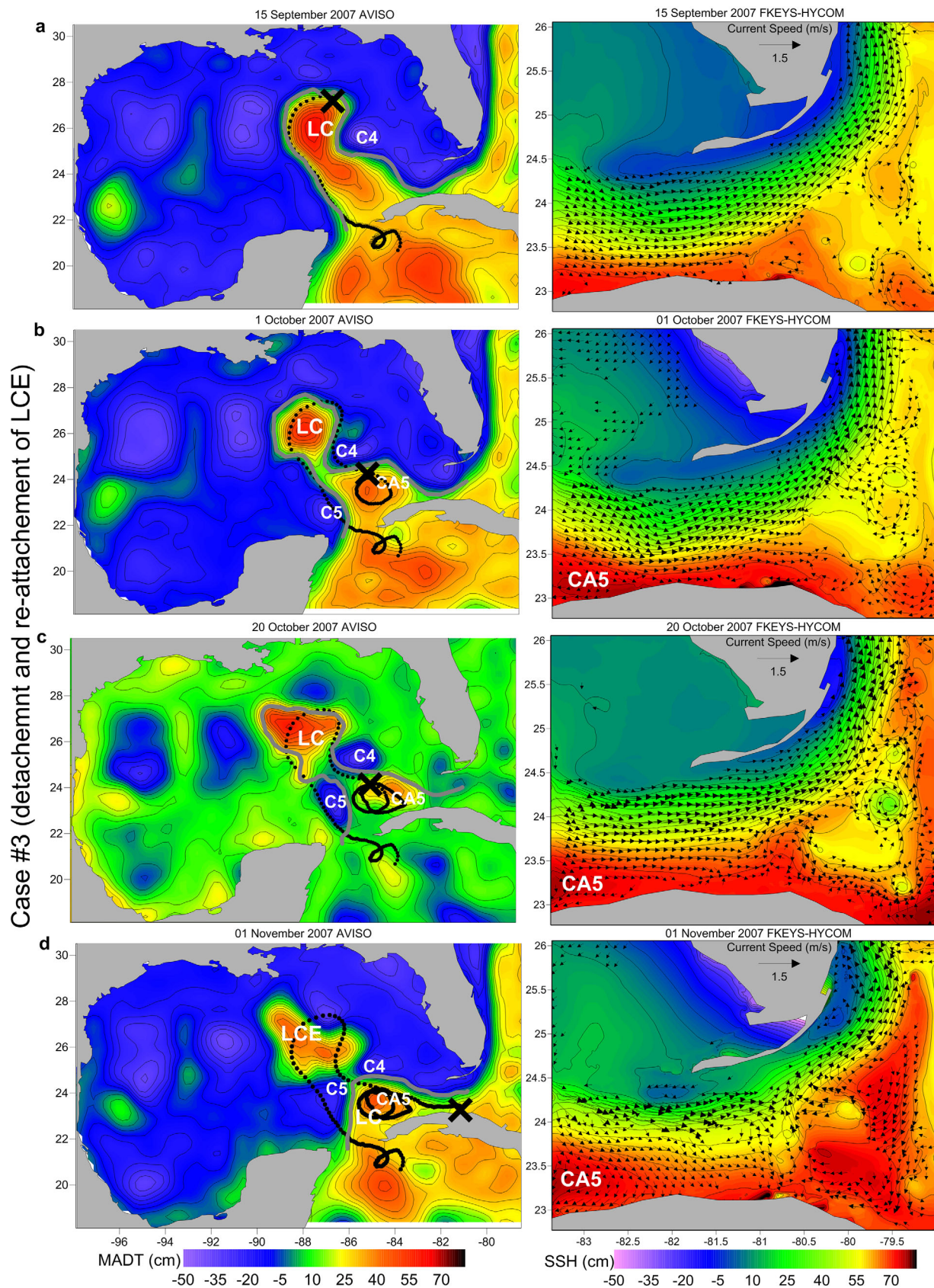


Figure 6. (continued)

the LC eastern side to first neck-down the LC and then keep the resulting LCE separated, favoring the CA5 enlargement inside the Straits of Florida. As the LCE became fully separated from the LC main body in the beginning of November, the CubAN's size increased, covering a large fraction of the northwestern Cuban coast (as far East as  $\sim 80.5^\circ\text{W}$  in the model; Figure 6d). The characterization of the CubAN velocity field and the quantification of the associated relative vorticity are presented in the Appendix; the relative vorticity is found to be between  $-0.1 f$  and  $-0.2 f$  ( $f$  the planetary vorticity) in the hypothesis of solid-body rotation.

Study Cases #2 and #3 illustrate how the CubAN presence along the Cuban coast is mainly associated with processes associated with LCE shedding that cover periods from the initial LC necking down to LCE detachments, reattachments and full separation that leads to a young LC phase over the western entrance of the Straits of Florida. As these processes are associated with the action of cyclonic LCFEs, these frontal cyclonic eddies may have an indirect contribution to the formation of the CubAN anticyclones. As shown in the Case #1 examples, the LCFEs can also have a direct effect on CubAN formation, by participating in the release of these anticyclonic eddies from the main LC body. The alongshore coastal circulation over the northwestern Cuba is strongly related to the presence of CubANs, which support intense westward flows, opposing those from the general eastward propagation of the FC.

#### 4.2. CubAN Evolution and Vertical Structure

Case #4 (Figure 7) presents the evolution of a CubAN (CA6) along the Straits of Florida in October 2012. The anticyclonic eddy was formed at  $\sim 83^\circ\text{W}$  in the beginning of October and was a part of a protracted CubAN formation period that lasted from June to November 2012. Very low LC latitude was observed during October, when the 17 cm contour, as derived from the AVISO altimetry, was detected around  $24.2^\circ\text{N}$ . A strong and extended cyclonic LCFE (C6) was located over the southeastern GoM, blocking the extension of the LC and keeping the young LC over the western entrance of the Straits of Florida (Figure 7a). The CA6 was already well formed by 5 October and continued to grow in size over the northwestern Cuban coast until 17 October (Figure 7c) without moving toward the east (type "A"), as derived from the simulated highest SSH contour. The contour lines in Figure 7c define the limits of an area where all SSH values close to the highest value within the eddy are included and the center of the eddy (dot) is defined by the highest SSH value within the eddy. The largest eddy size of CA6 occurred on 25 October, when the highest SSH ( $\sim 75$  cm contour, encompassing all SSH values close to 75 cm) covered a large area with a diameter of approximately 100 km. The center of the eddy shifted eastward, indicating that the eddy evolved into a type "B" CubAN, and started to propagate along the Cuban coast. Its maximum SSH dropped by about 15 cm at  $82^\circ\text{W}$  at the end of October (down to  $\sim 60$  cm), indicating a weakening of the eddy, as it was drawing away from the LC body. Finally, the eddy size was decreased when it reached the eastern part of the region by 3 November. At that time, a new but smaller CubaN (CA7) formed over the western region (5 November), suggesting that CubANs start growing from a relatively small size during their initial phase (close to the  $\sim 30$  km diameter mesoscale threshold). The cycle of the CA6 CubAN lasted  $\sim 1$  month (October 2012), evolving from type "A" to type "B" CubAN, as it was advected eastward.

The evolution of the Mixed Layer Depth (MLD) within the CubAN's core during October 2012 (Case #4) is shown in Figure 7d. The sigma-t ( $\sigma_t$ ) criterion was used to determine the depth where the  $\sigma_t$  density is equal to the surface  $\sigma_t$  value plus the increment in density equivalent to a specific decrease in temperature ( $\Delta T$ ).  $\Delta T$  is set equal to  $0.3^\circ\text{C}$ , and salinity is constant and equal to the sea surface salinity. The MLD is computed by detecting the depth where  $\sigma_t$  is equal to the surface  $\sigma_t$  plus the density difference from the surface to the base of the MLD (MLD criterion by Felton et al., 2014). The MLD reveals its shallowest value during the formation of the CA6 CubAN in the beginning of October ( $< 20$  m). The MLD increased during the CA6 evolution over the western region until 25 October, revealing a 55 m homogeneous upper layer in the core of the eddy. Although the SSH reduction on 29 October temporarily blocked the MLD increasing trend, the

**Figure 6.** Case #3—Maps of (left) AVISO Mean Absolute Dynamic Topography (MADT) and (right) FKEYS-HYCOM Sea Surface Height (SSH) and current vectors (m/s) during a young Loop Current (LC) phase characterized by detachment and reattachment of LC Eddy, LCE: (a) 15 September 2007, (b) 1 October 2007, (c) 20 October 2007, and (d) 1 November 2007. The LC and LCE location (17 cm SSH contour, grey line), the major cyclones (C), and the CubANs (CA) are indicated on each map. "X" symbols mark the drifter #70325 position around the dates of the corresponding sea level field. The black dots mark the drifter position in previous days.

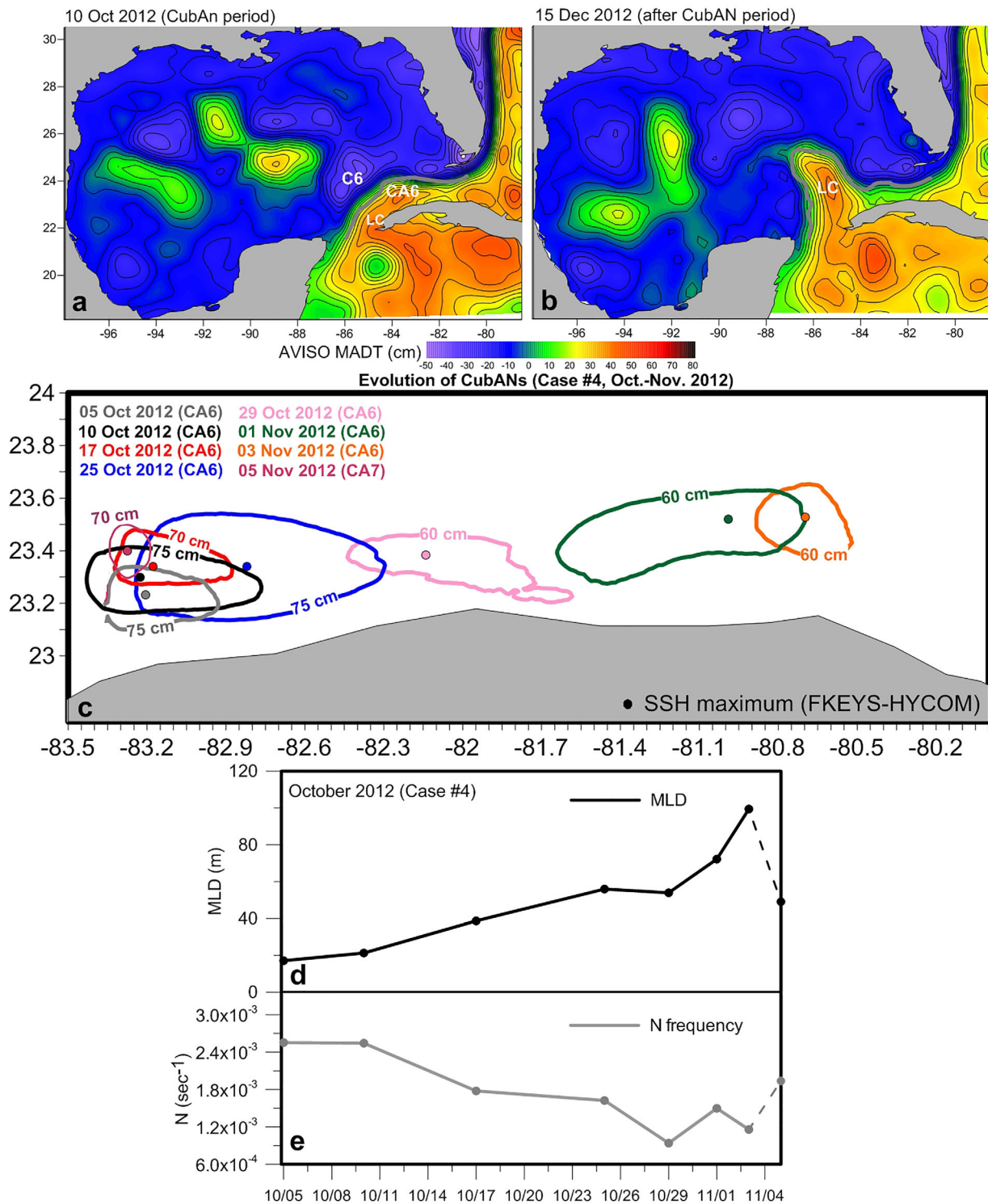


**Figure 7.** Case #4—Maps of AVISO Mean Absolute Dynamic Topography (MADT) for (a) 5 October 2012 (during the CubAN period) and (b) 15 December 2012 (after the CubAN period). The Loop Current (LC, 17 cm contour, grey line), the major cyclone (C6), and the CubAN (CA6) are indicated on each map. (c) Several snapshots of the CA6 evolution along the Cuban coast in October 2012, as derived from the simulated (FKEYS-HYCOM) Sea Surface Height (SSH) fields. The formation of the CA7 CubAN on 5 November 2012 is also presented. The center (maximum SSH) of the CubAN for each date is indicated with a respective colored dot. (d) Mixed Layer Depth (MLD, m) and (e) N stratification frequency ( $s^{-1}$ ), averaged over the upper 100 m along the CubAN track during October 2012. The dots indicate the date of the CubAN's center presented with dots in Figure 7c. The solid lines indicate the evolution of the CA6 CubAN, and the dashed lines indicate the formation of the following CA7 CubAN on 5 November 2012.

evolution into a type “B” CubAN along the Cuban coast was associated with an additional MLD increase until 3 November.

The reduction of the  $N$  stratification frequency (Brunt-Väisälä frequency), averaged over the upper 100 m at the CA6 core (Figure 7e), is associated with the formation of a thicker mixed layer inside the eddy. The  $N$  frequency was around  $0.0026 \text{ s}^{-1}$  on 5 October 2012, but was gradually reduced down to  $0.0016 \text{ s}^{-1}$  by 25 October. The evolution of the CA6 into type “B” and its propagation along the Cuban coast at the end of October and in the beginning of November were followed by a strong increase of the MLD, reaching its largest level ( $\sim 100 \text{ m}$ ) west of  $81^\circ\text{W}$  on 3 November. The respective stratification frequency during its propagation along the coast ranged from  $0.001$  to  $0.0015 \text{ s}^{-1}$ , confirming the weak stratification in the eddy core. The formation of the young CA7 CubAN over the western region on 5 November (Figure 7c) is associated with a lower MLD ( $\sim 40 \text{ m}$ ) and a respective higher stratification frequency ( $\sim 0.0018 \text{ s}^{-1}$ ). The formation of the type “A” CubAN and evolution into a moving type “B” CubAN are related to increasing MLD and weaker upper ocean stratification along the eddy track.

Case #5 (Figure 8) took place during the long CubAN period of 2016, which lasted from mid-spring to winter with significantly low LC and high FC zonal positions (Figure 4). Two CubANs (CA8 and CA9) are detected in early-August 2016 off the northwestern Cuban coast. A small cyclonic eddy (C7), associated with the strong FC curvature, is also detected between the two CubANs at  $83.5^\circ\text{W}$  (lower SSH values). CA8 is a type “A” eddy and CA9 propagates toward the East, showing type “B” characteristics in mid-August. Drifter #145522 was trapped in the CA8 eddy on 13 August after its northward propagation along the Yucatan Channel and its intrusion in the Straits of Florida. The location of the drifter trajectory and the amplitude of its anticyclonic loops agree well with the model SSH and current patterns, confirming the ability of the model to represent CubAN eddies in a realistic manner. The low drifter speeds inside the eddy ( $<0.5 \text{ m/s}$ ) agree with the

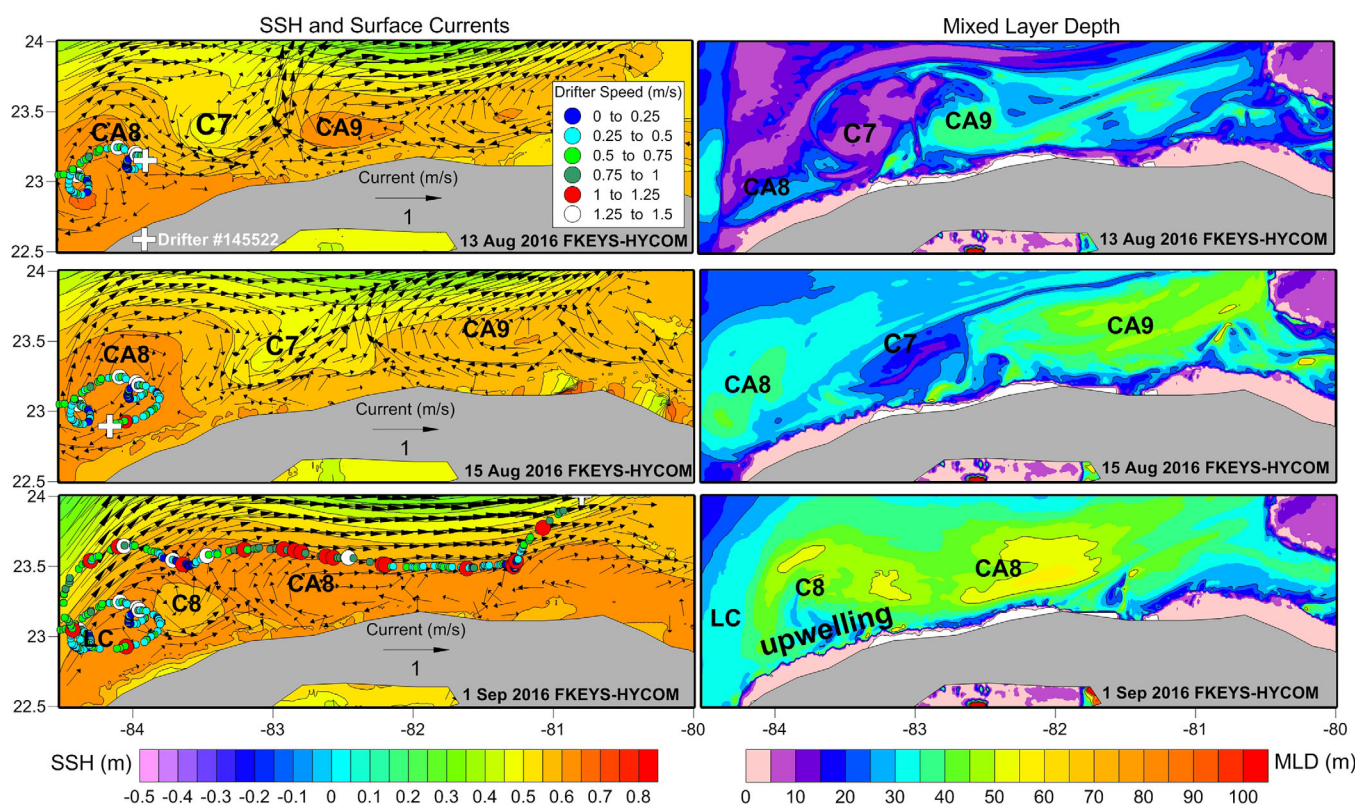


**Figure 8.** Case #5—Maps of (left) Horizontal distribution of Sea Surface Height (SSH) and surface currents and (right) Mixed Layer Depth (MLD) derived from the FKEYS-HYCOM simulation on (top to bottom) 13 August 2016, 15 August 2016, and 1 September 2016. The CA8, CA9, C7, and C8 eddies, the Loop Current (LC), and the upwelling area along the northern Cuban coast are presented. Trajectory of drifter #145522 along the Straits of Florida is marked on the SSH plots (the white cross indicates the drifter’s position during each SSH snapshot); circle colors denote drifter speed (in  $\text{m s}^{-1}$ , values in the box insert); speeds over  $1 \text{ m s}^{-1}$  (red and white) are marked by larger circles.

simulated currents in magnitude and direction (southward on 13 August and westward on 15 August). This result agrees with the drifter trajectories and speeds presented in Appendix Figure A1, when the drifter speed levels were significantly reduced after the entrainment of the drifter inside the anticyclonic eddy. The MLDs of the three eddies are also presented in Figure 8. CA9 shows thicker mixed layer than CA8 on 13 August 2016, in agreement with the Case #4 findings. CA9 moved eastward by 15 August and its MLD deepened to 50 m, covering an extended area off northern Cuba. The MLD of CA8 also deepened from 30 to 45 m over these 2 days. The following 15 days were characterized by the evolution of CA8 to a type "B" CubAN with a deeper mixed layer (~60 m). This CubAN significantly increased in size and reached the central region along the northwestern Cuban coast in the beginning of September. The C7 cyclonic eddy revealed shallower MLD on 13 and 15 August and it totally disappeared by 1 September. The formation of another cyclonic eddy (C8), located over the northwestern tip of Cuba, is discussed in detail in section 4.4. The drifter eastward trajectory was characterized by higher speeds ( $>0.75$  m/s) due to the strong eastward currents of the FC; respective strong surface currents were simulated by the model along the front between the northern part of the anticyclonic CA8 eddy and the FC. The drifter propagated along this front before its offshore northward removal later in September. For more information about CubAN dynamics based on drifter data see the Appendix A.

Study Cases #4 and #5 show that CubANs reveal weaker currents than the LC core, with strong variation between their northern and southern part. Strong variation was also detected in their stratification, mixed layer, and size characteristics during their evolution from type "A" to type "B" eddies.

#### 4.3. Influence of CubANs on Alongshore Transport

Figure 9 presents the mean transport along section  $S_1$  (marked on Figure 1) and the corresponding evolution of the FC zonal position (taken as the position of the  $20^\circ\text{C}$  isotherm at 150 m along the  $83^\circ\text{W}$  meridian; as in Kourafalou & Kang, 2012). The 2004 zonal transport along the Cuban coast during the presence of CA1 (Case #1, Figure 5) showed a significant drop toward negative values at the end of April ( $-1$  Sv), indicating a strong westward current across this section, in the southern part of the anticyclonic CA1 eddy. Prior to that, the strong eastward transport along the coast on 1 April (2 Sv) indicated the absence of anticyclonic activity, as the eastward moving FC was at a southward position, near Cuba. The FC position and the alongshore transport are thus anticorrelated, as also confirmed by the high negative Pearson coefficient between both time series ( $r_{2004} = -0.66$ ). The strongest eastward transport occurred during the most southern positions of the FC. On the contrary, strong westward transport along the Cuban coast usually occurred when the FC front was detected at higher latitudes, away from the Cuban coast (as in Case #1). The end of the CubAN period in May 2004 was followed by an eastward transport along  $S_1$  (1.5 Sv), and a southward shift of the FC ( $\sim 23.5^\circ\text{N}$ ). This study case is related to the cyclonic activity (C2, Figure 5) along the extended LC over the central GoM, which activated the formation of a type "B" CubAN by initiating a curvature at the eastern part of the LC, off northwestern Cuba.

Similar to Case #1, the Case #2 CubAN eddies (Figure 5) are associated with strong westward transports along the Cuban coast (Figure 9, 2004), where a large negative value was computed across section  $S_1$  ( $-1.6$  Sv) in June, following the clear eastward currents of the previous month (1.6 Sv). The FC front shifted toward the North, leading to its most northern position in 2004 ( $\sim 24.3^\circ\text{N}$ ). The CA2 and CA3 CubANs caused westward transport, with a brief interruption around 1 June, caused by the small cyclone discussed in section 4.1. When the FC was near Cuba (as in Case #3, Figure 6), strong eastward transport was evident along the Cuban coast (1.8 Sv; Figure 9, 2007) and the correlation coefficient with the FC position was large and negative ( $-0.72$ ). The extended period of the CA5 CubAN along the Cuban coast is reflected on the long period of westward transport across section  $S_1$  in October and November. The peak of the westward transport occurred in mid-November ( $\sim -1$  Sv), when CA5 occupied a large area along the coast. The transport reversed and showed positive high values in December ( $\sim 1.7$  Sv), when the FC assumed a central position in the Straits of Florida ( $23.7^\circ\text{N}$ ; Figure 9).

During Case #4 (Figure 7), the 2012 transport (Figure 9) was influenced by a long period of CubANs presence, during which several successive pulses of westward transport occurred from June to November. The presence of the CA6 type "A" CubAN caused the strongest westward transport of the year in October ( $\sim 1.3$  Sv). The FC front experienced a northward displacement in the Straits of Florida during this 6 month period, following a southern position in spring. The correlation coefficient is negative ( $-0.57$ ), in agreement with

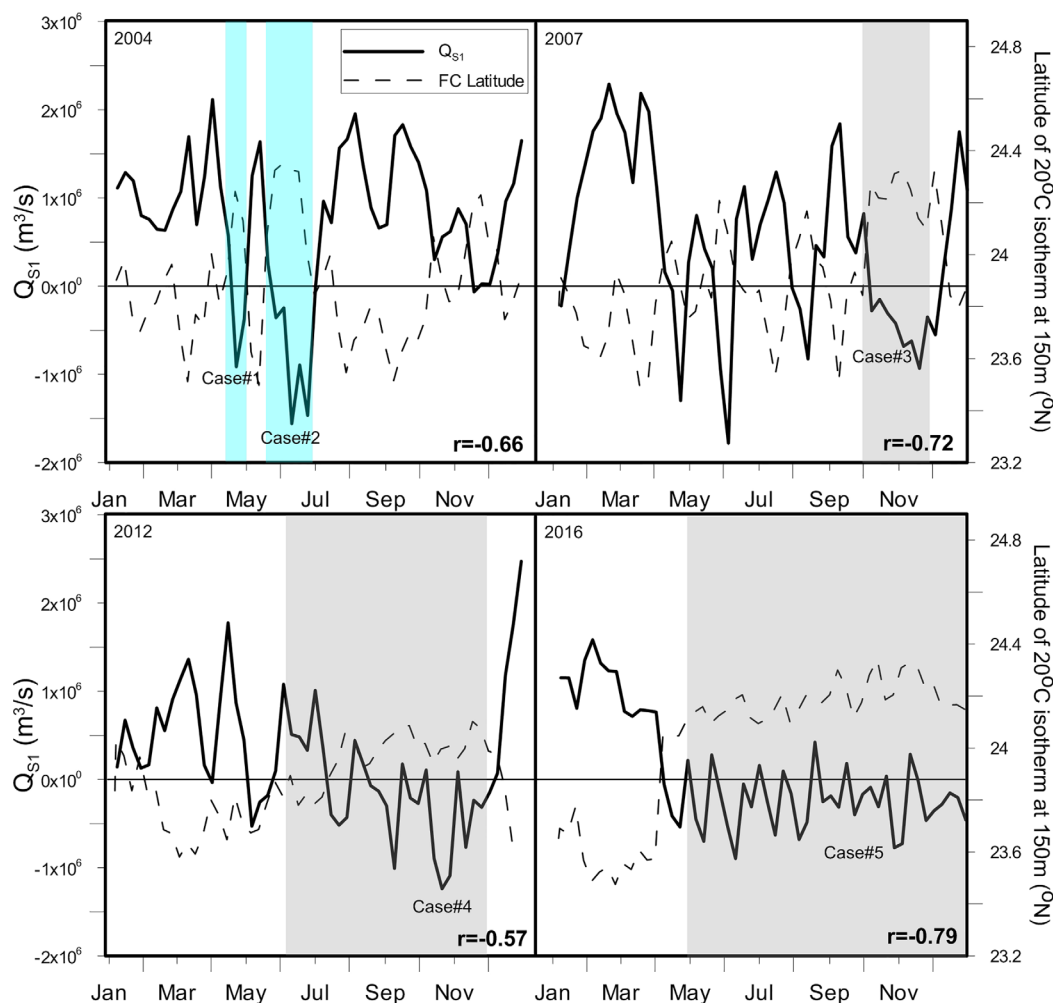


**Figure 9.** Weakly mean transport ( $Q_{S1}$ ,  $m^3/s$ ) across section  $S_1$  (marked on Figure 1), derived from the FKEYS-HYCOM simulation and averaged over the upper 100 m for the years 2004 (Case #1, Case #2), 2007 (Case #3), 2012 (Case #4), and 2016 (Case #5). Positive and negative values correspond to eastward and westward direction of the transport, respectively. The dashed lines indicate corresponding evolution of the Florida Current (FC) zonal position ( $20^\circ C$  isotherm at 150 m along  $83^\circ W$ ). The correlation coefficients between the daily transport and FC time series are also presented for each year. The shaded areas indicate the periods when the five study cases (Table 1) of formation and evolution of CubANs occurred (grey during Loop Current, LC, low latitude and cyan during LC high latitude).

the previously noted anticorrelation between the FC position and the alongshore transport across section  $S_1$ . The entire Case #5 period (Figure 8) is characterized by successive episodes of westward transport along the CubAN coast (Figure 9, 2016), due to the formation and evolution of several CubANs (Figure 4). Although the transport is highly variable, it remains mostly negative (westward), with values reaching  $\sim -1$  Sv. The highest correlation ( $r_{2016} = -0.8$ ) between the FC position and the alongshore transport at  $S_1$  was computed in 2016.

#### 4.4. Eddy Interaction With Wind-Induced Upwelling

We showed that CubANs may induce a strong alongshore current that promotes westward transport, opposing the prevailing eastward FC transport. Another important effect of these warm-core anticyclones is the potential to significantly increase the coastal temperature. On the contrary, SST reductions are expected due to the prevailing easterly winds over northern Cuba (especially during summer) that are upwelling favorable (Rossov & Santana, 1966). We examine the interaction between CubAN evolution and upwelling processes during two strong upwelling events (June 2004 and August 2016).

The upwelling-favorable wind conditions in June 2004 are evident in Figure 10a, during the presence of Case#2 CubANs CA2 and CA4 (Figures 10b and 10c; see also Figures 5c and 5d). The GHR SST horizontal distribution (Figure 10d) reveals cooler waters (<28°C) over an extensive coastal area, surrounded by preexisting warmer masses (~29°C). The upwelled waters are also identified by the respective ocean color distribution (Figure 10e), in the form of distinct filaments, as more productive waters (higher chl *a* content) were present over the surface layers on the same day. These waters were advected offshore and they propagated between the fronts of CA2 and CA4. We deduce that the appearance of upwelled cooler waters contributed to the separation of a type “A” CubAN (CA2) from the LC core and the subsequent separation of an eastward moving type “B” CubAN (CA4). The two eddies and the upwelled waters separating them are evident in both GHRSTT and ocean color data.

Strong eddy activity along the Cuban coast was also simulated in the beginning of September 2016, forming a distinctive cyclonic eddy (C8) in the west side of CubAN CA8. The formation of the CA8 and CA9 CubANs in August 2016 (Case #5, see also Figure 8) is followed by a temperature increase over the

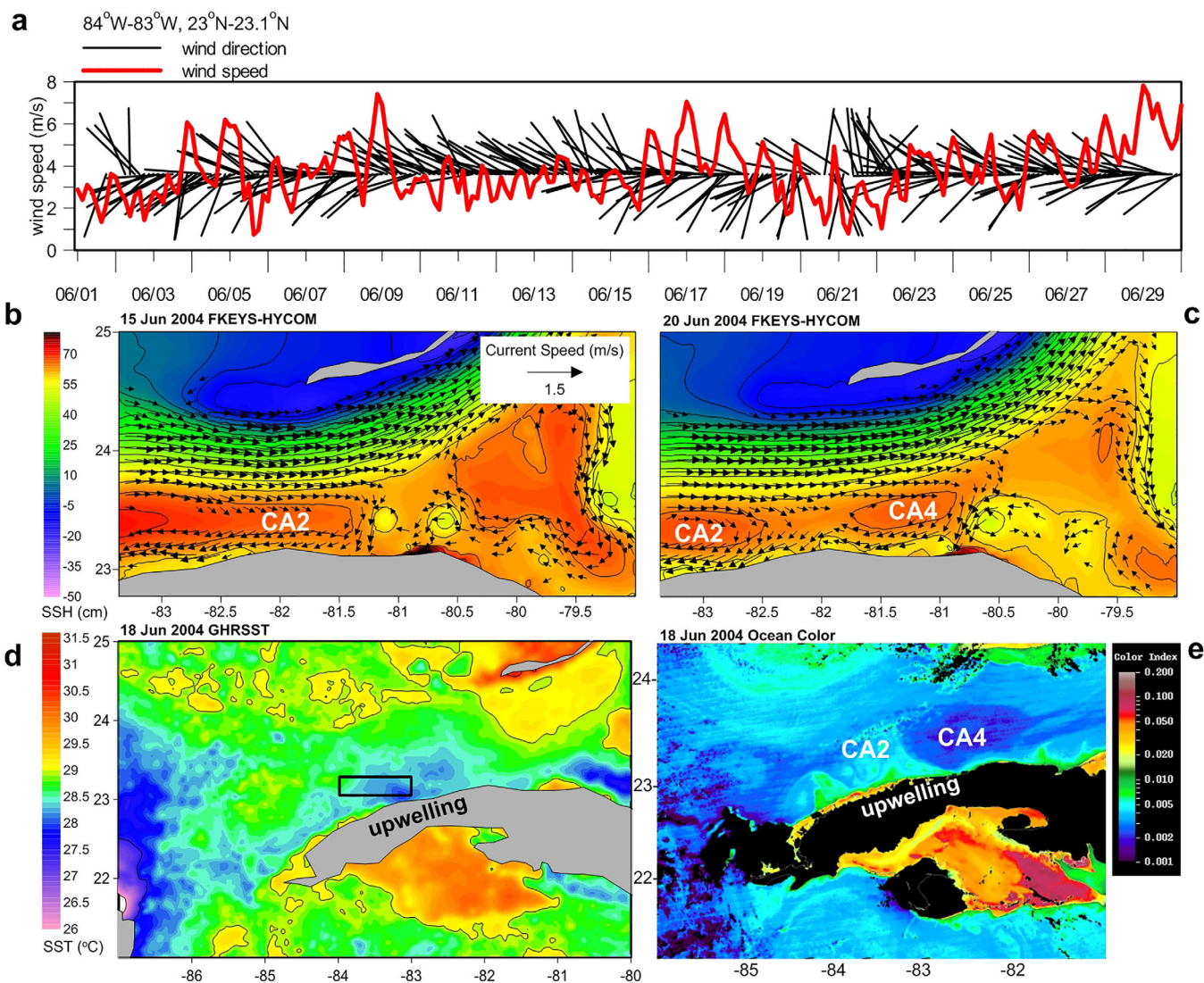


**Figure 10.** Evolution of (a) 3-hourly wind speed and direction (COAMPS) during June 2004 (Case #2) period (note that all direction sticks have same length), averaged over the 84°W–83°W and 23°N–23.1°N region (box marked in bottom-left plot). Maps of horizontal distribution of Sea Surface Height (SSH) and surface currents (FKEYS-HYCOM) on (b) 15 June 2004 and (c) 20 June 2004, (d) Sea Surface Temperature (SST, GHRSTT data), and (e) satellite ocean color on 18 June 2004. The CA2 and CA4 eddies and the upwelling area along the northern Cuban coast are presented. “Upwelling” marked over the Cuba land mass indicates upwelling area near the coast (marked by cooler/blue color waters in GHRSTT data and more productive/green color waters in ocean color data).

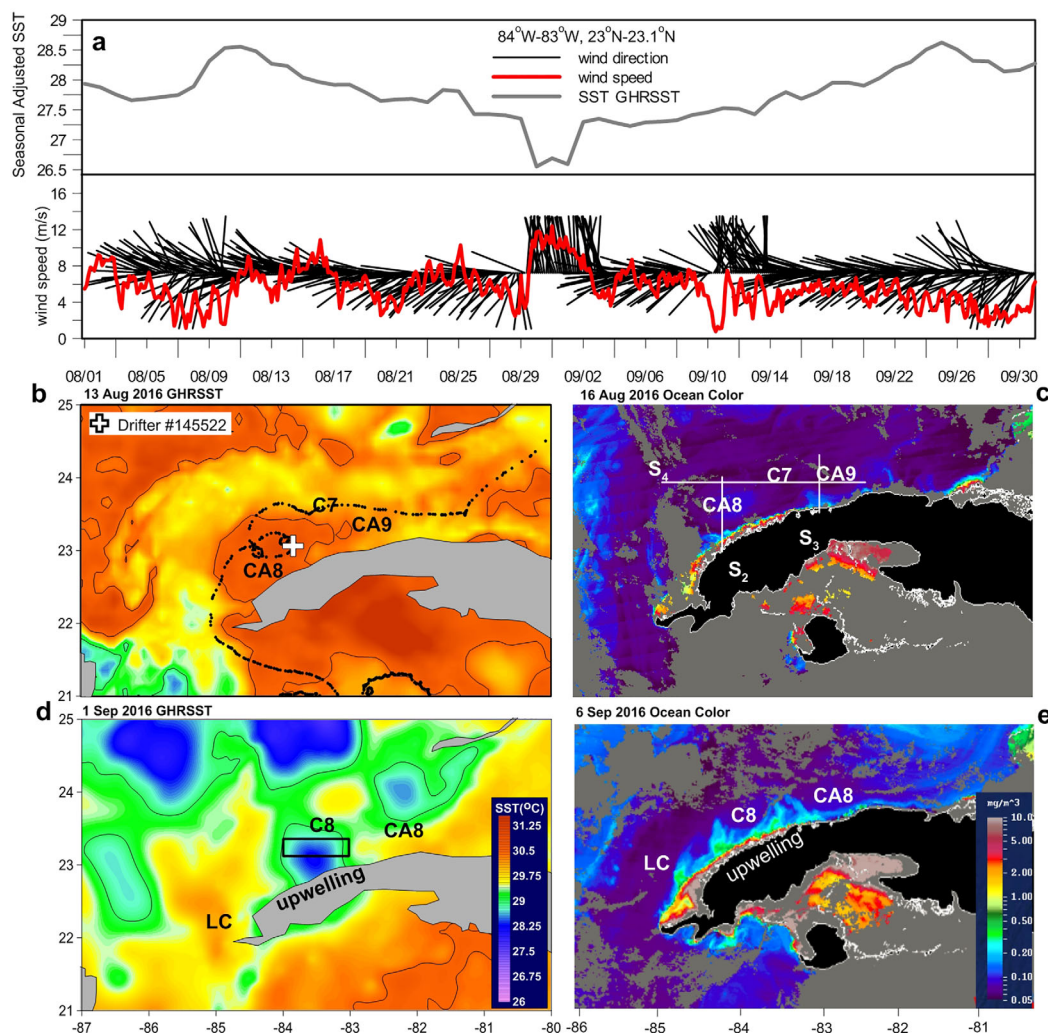


**Figure 11.** Evolution of (a) daily Sea Surface Temperature (SST, GHRSSST data) and 3-hourly wind speed and direction (NAVGEM) during August–September 2016 period (note that all direction sticks have same length), averaged over the 84°W–83°W and 23°N–23.1°N region (box marked in bottom-left plot). Maps of horizontal distribution of (b) SST (GHRSSST) and (c) satellite ocean color in mid-August and the respective (d) SST and (e) ocean color in early-September. The evolution of the drifter #145522 (black dots) and its position on 13 August 2016 (cross) are also presented. The CA8, CA9, C7, and C8 eddies, the Loop Current (LC), and the upwelling area along the northern Cuban coast are presented. The solid white lines indicate sections  $S_2$  (84°W, 22.7°N–23.25°N),  $S_3$  (83°W, 23°N–23.6°N), and  $S_4$  (23.2°N, 84.5°W–82°W) used in Figure 13. “Upwelling” marked over the Cuba land mass indicates upwelling area near the coast (marked by cooler/blue color waters in GHRSSST data and more productive/green color waters in ocean color data).

northwestern Cuba region. The observed SST, averaged over the area between 83°W to 84°W and 23°N and 23.1°N, revealed a peak (28.5°C) around 11 August, due to the presence of anticyclonic eddies over the area (Figure 11a). High SST values were observed when drifter #145522 was entrapped inside the CA8 anticyclonic eddy, right after its intrusion in the Straits of Florida (13 August; Figure 11b). The respective ocean color distribution also confirms the presence of the two CubAN eddies (Figure 11c); the eddy fronts are characterized by filaments of higher chl *a* concentrations. During this eddy activity, easterly winds triggered upwelling along the Cuban coast. The weak offshore spreading of the upwelled waters contributed to the small SST reduction until 29 August (27.25°C), when a much bigger SST drop was observed (Figure 11a). This was associated with intense southerly winds from Tropical Storm Hermine (Berg, 2017), which lasted from 29 August 2016 to 3 September 2016. The upwelled, cooler coastal waters were advected offshore, resulting in substantial cooling over an area between 84°W and 83°W (Figures 11d and 11e). This cooling was also supported by the removal of the CA8 warm-core CubAN eddy, which moved eastward. This shift

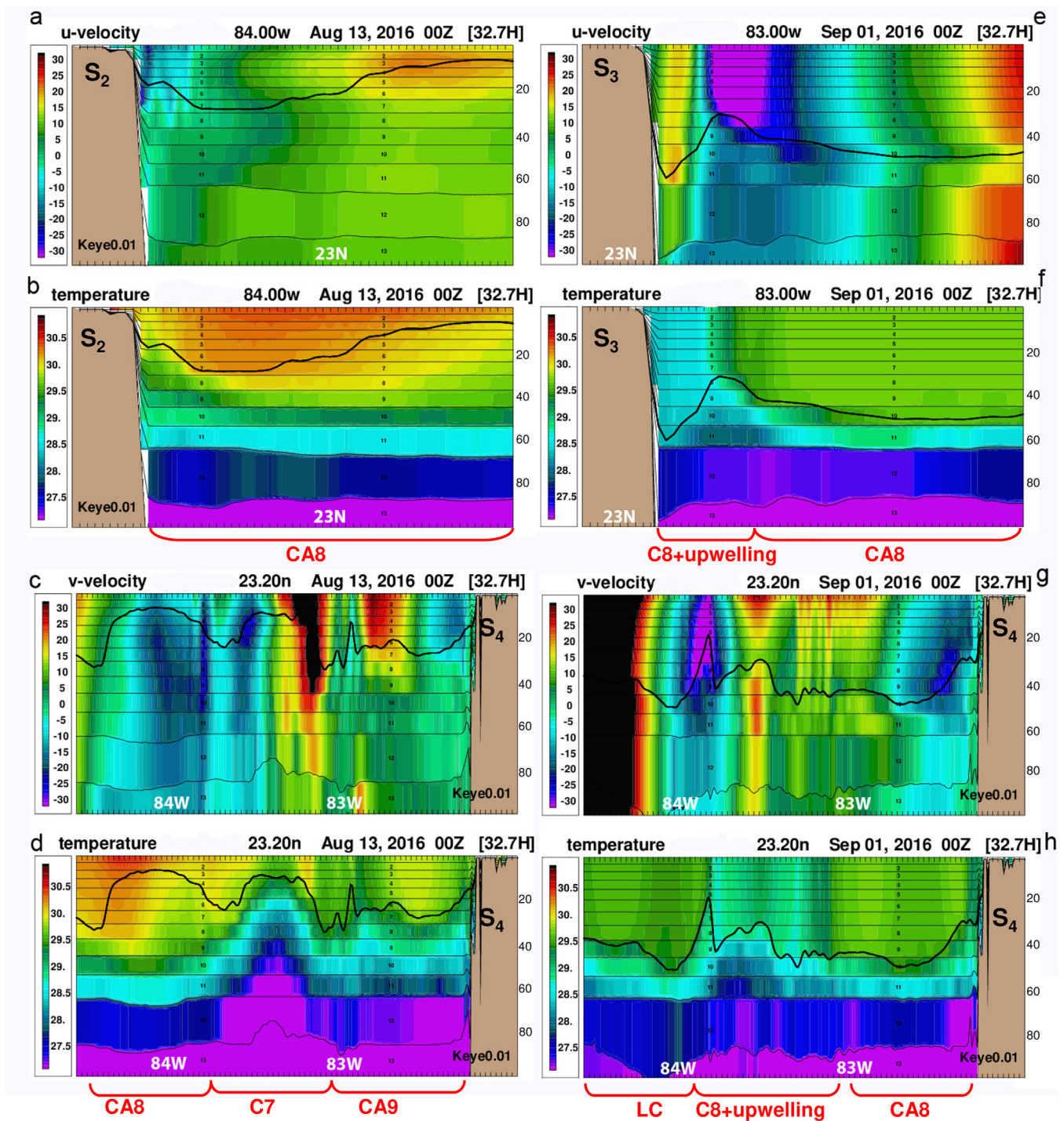


**Figure 12.** Cross-sectional distribution of (a, e) zonal velocities (eastward: positive; westward: negative) and (b, f) temperature over the upper 100 m of section  $S_2$  (13 August 2016) and section  $S_3$  (1 September 2016; Case #5). Cross-sectional distribution of (c, g) meridional velocities (northward: positive; southward: negative) and (d, h) temperature over the upper 100 m of section  $S_4$  (13 August 2016, 1 September 2016). The Mixed Layer Depth (MLD, m, black solid line) and the major physical processes (CA8, CA9, C7, C8, upwelling, Loop Current [LC]) are also indicated. Sections are marked on Figure 11c.

was presumably connected to the formation of a cold-core cyclonic eddy (C8), over the upwelling area around 1 September (Figure 8). The cooler waters marked an extended upwelling region of about 10,000 km<sup>2</sup> on 1 September (Figure 11d); the round shape of the cooler/blue pattern on the GHRSSST observations on 1 September is consistent with the presence of the C8 cyclone. The upwelled waters are also

detected in the ocean color images, as more productive waters spread offshore, along the fronts of both cyclonic C8 and anticyclonic CA8 eddies (6 September; Figure 11e).

Figure 12 shows model computed meridional and zonal current velocity and temperature, along sections  $S_2$ ,  $S_3$ , and  $S_4$  (marked on Figure 11). In mid-August 2016, the anticyclonic CA8 CubAN caused stronger eastward velocities offshore ( $>25$  cm/s at the upper 20 m) and weaker westward current along the coast ( $\sim 15$  cm/s over the upper 40 m); Figure 12a. The temperature section had a warm area associated with CA8 (Figure 12b). At the same time, the highest ( $>25$  cm/s) northward velocities (Figure 12c) are seen around  $83^\circ\text{W}$ , where the western front of the CA9 anticyclonic CubAN was adjacent to the C7 cyclonic eddy that formed between CA8 and CA9 (Figure 8). The temperature field (Figure 12d) reflects the upwelling process in the core of the cyclonic eddy. Deeper cooler waters reached the surface and a cone-shape temperature distribution with lower temperatures was observed between the two CubANs ( $\sim 83.5^\circ\text{W}$ ). The highest temperature values were observed inside CA8 ( $\sim 30^\circ\text{C}$ ), covering the upper 40 m of the water column, especially over the southern part of the eddy, where the MLD shows its deepest values ( $\sim 25$  m; Figure 12a). The water column inside CA8 is completely stratified below 50 m, indicating that the CubAN structure along the coast affects the upper 50 m of the ocean, dominating the stratification frequency reduction over the upper 100 m presented in Figure 7e.

The evolution of current and temperature structure was dominated by the succession of warm-core anticyclones, cold-core cyclones and upwelled waters. A second cyclonic eddy (C8) was formed along the Cuban coast by the beginning of September 2016 (Figures 12e and 12f) and separated two anticyclonic features: the LC and the CA8 CubAN, which advanced eastward (Figure 12g). The strong northward velocities at  $83^\circ\text{W}$  due to the synergy of C8 cyclone, CA8 anticyclone and strong southerly winds caused the offshore advection of the cooler surface waters (Figure 12h), spreading them along the eddy-induced fronts (Figure 11). The upwelling period of August–September was the only case of significant reduction of seasonally adjusted SST along the Cuban coast during the 2016 CubAN period (Figure 3a). The cyclonic activity under the combination of wind-induced upwelling processes, the strong tropical storm winds and the formation of the C8 cyclonic eddy played an important role on the separation of the CA8 anticyclone from the LC body and its evolution to a propagating type “B” CubAN along the Cuban coast.

## 5. Summary and Conclusions

Novel processes have been discussed in the southeastern Gulf of Mexico and the Straits of Florida, specifically the formation and evolution of mesoscale anticyclonic eddies along the northern Cuban coast (CubAN eddies). The study reveals a synergy between the overall evolution of the LC/FC system and CubAN eddies, in addition to the previously known interactions of this current system with its related cyclonic frontal eddy field. In particular, CubANs were associated with: (a) periods of anticyclonic LCE detachment, which eventually leads to a retracted LC near Cuba, and (b) the FC undulations within the Straits of Florida.

The identification and investigation of CubAN eddies are supported by both high-resolution simulations and observations (satellite, drifter, and buoy data). Although the high-resolution FKEYS-HYCOM simulation does not assimilate observations, it showed good agreement with the observations during a prolonged study period (2004–2016). The presence of warm-core CubAN anticyclones influenced SST patterns within the Straits of Florida. The seasonally adjusted SST showed a clear general increase during the 13 year period with a shift in the fall of 2013, when the mean SST increased by more than half degree. This increase coincided with protracted periods of warm anticyclonic CubAN presence. Significantly high occurrence frequency of CubANs was found in 2013. The highest temperature levels were simulated and observed in 2016, when the largest number of CubANs evolved in the Straits of Florida, along the Cuban coast, supporting the general trend of SST increase during the entire study period. Satellite altimetry data, drifters, and ADCP measurements also supported the model's efficiency to incorporate the effects of the regional circulation patterns in the evolution of mesoscale dynamics inside the Straits of Florida and to advance the understanding of important dynamics, especially the role of cyclonic (anticyclonic) activity to the north (south) of the FC front.

Two types of CubAN eddies have been described: (a) a main anticyclonic eddy (type “A”) within the core of the LC over the northwestern tip of Cuba, which usually takes place during the LCE shedding process and when the LC is retracted (young LC phase), and (b) a distinct anticyclonic eddy that is released from the

main LC core and is advected eastward, along the northern Cuban coast (type "B"). A type "A" CubAN can also be present in tandem with one or more eastward progressing type "B" eddies.

CubAN eddy activity coincides with northern displacements of the FC in the Straits of Florida. An anticorrelation between the north-south shift of the LC and the FC meridional position was computed, with the CubAN activity favored during southern LC position. The majority of the anticyclonic eddy activity along the northwestern Cuban coast is triggered by the onset of necking down conditions of the LC (under cyclonic LC frontal eddy influence) that is followed by LCE detachments, reattachments and full ring separation. The cyclonic eddies traveling along the LC and FC fronts (clockwise around the LC and north of the FC) may also contribute to the formation of CubANs, either indirectly by participating in the shedding events of the LCE (type "A" formation), which is their most common contribution, or in some cases directly, by participating in the release of CubANs from the main LC core over the northwestern tip of Cuba (type "B" formation). A feedback from the CubANs to the FC undulations in the Straits of Florida was found, extending results from previous studies that associated FC meandering with cyclonic eddy activity to the north of the FC front. We conclude that the FC is influenced by both cyclonic frontal eddies along the South Florida and the Florida Keys and CubAN anticyclonic eddies along the Cuban coast. Furthermore, CubAN activity can lead to the northward displacement of the LC/FC front at the western entrance of the Straits of Florida, near the Dry Tortugas and the Southwest Florida Shelf escarpment. Strong correlation between the FC meandering and the evolution of CubANs was detected along the Straits. As shown by Kourafalou and Kang (2012), this can lead to local formation of cyclonic eddies, when shelf circulation conditions are favorable (westward to southward currents). This amplifies the FC curvature and can potentially further support the conditions that favor CubAN presence.

The eastward advection of CubANs was found related to the presence of cooler coastal waters by the base of the LC core that were associated with wind-driven upwelling and cold-core cyclonic eddies. These cooler waters were found to separate CubANs type "B" from those of type "A" and facilitate their eastward advection (which could last a few weeks). On average, CubAN eddies were found present almost one third of the year, with higher occurrence frequencies during summer. The conditions behind this seasonality are not clear yet. We suspect it is related to the prevailing coastal upwelling processes that usually occur during summer, but more detailed investigation is needed and it will be the subject of future studies.

The highest eastward transport rates along the northwestern Cuba occurred during the most southern positions of the FC. However, the CubAN presence introduces strong westward coastal currents, opposing the general FC transport. Drifter and model analysis showed that the currents of the extended LC are generally stronger than the currents within a CubAN anticyclonic eddy. Moreover, the westward currents over the southern part of a CubAN are weaker than the eastward currents over its northern part, which is usually adjacent to the LC/FC system. However, these are locally strong coastal flows that can substantially enhance the prevailing westward wind-driven circulation along the narrow northern Cuba shelf. The CubANs can also provide pathways for cross-shelf transport. The detailed analysis of a drifter trajectory provided an estimate of the relative vorticity of the sampled CubAN eddy, which is found to be between  $-0.1 f$  and  $-0.2 f$  ( $f$  the planetary vorticity) in the hypothesis of solid-body rotation. More observations are needed to assess the vorticity budget of CubAN eddies.

The evolution of a type "A" to a propagating type "B" CubAN is further associated with a respective mixed layer deepening, a size increase, and a stratification weakening of the upper ocean along its eastward track. The presence of CubAN eddies affects especially the upper 50 m of the water column, increasing the temperature levels. In combination with adjacent cooler waters due to wind-induced coastal upwelling and cold-core cyclonic eddies, strong temperature gradients are formed over northern Cuba waters, which may have substantial effects on reefs and Marine Protected Areas. Implications can be broader on the connectivity of GoM ecosystems, as new studies are under way to study Cuban coral reefs (as the Guanahacabibes National Park, near the northwestern tip of Cuba), in connection with U.S. National Marine Sanctuaries, including the Florida Keys and the Dry Tortugas (U.S. and Cuba Memorandum of Understanding, 2015). The better understanding of the interconnection between these ecologically important regions is also dictated by oil exploration efforts along northwestern Cuba that started in recent years.

The present study offers a definition of the CubAN eddies and illustrates several study cases, revealing common aspects and variability related to their detection. Study analyses establish observational

and modeling evidence of these mesoscale anticyclones along northwestern Cuba for a period of 13 years, quantifying favorable conditions for their formation and evolution, as well as their interaction with the overall mesoscale circulation in the Gulf of Mexico and the Straits of Florida. As new observations in the study area become available, further analyses on the dynamical mechanisms controlling the formation and evolution of the CubAN eddies will be possible. Furthermore, the tendency for increasing number of warm CubAN eddies over the study period can be possibly employed to explain the increasing SST within the Straits of Florida. Studies over longer time scales would be necessary to further associate with the overall variability of the Loop Current, Florida Current, and Gulf Stream modulations.

### Appendix A: CubAN Dynamics Based on Drifter Data

We employ the data from drifter #70325, which sampled the Case #3 CA5 CubAN eddy (Figure 6), to quantify the eddy characteristics, particularly its propagation speed and relative vorticity. The two anticyclonic loops of the drifter inside the CubAN eddy are presented in detail in Figure A1. The drifter speed was high ( $>4$  km/h; Figure A1a) during its propagation along the LC front in September, when the LC was significantly extended inside the GoM (Figure 6a). The movement of the drifter inside the CubAN at the end of September (Figure A1a) was followed by a speed reduction down to 2 km/h. This suggests that the currents along the front of an extended LC could be significantly stronger than the currents of an anticyclonic type "A" CubAN. The westward propagation of the drifter over the southern part of the vortex between 22 and 26 September is characterized by even lower velocity down to 1 km/h. The drifter speed increased along the northward and eastward propagation from 27 September until 5 October, when it was adjacent to the LC/FC system. However, its second spin inside the eddy is characterized by one more speed reduction during its southward and westward transport (6–15 October). Finally, the drifter speed increased to 2 km/h after 15 October, reaching its highest levels during its presence in the Straits of Florida by 25 October ( $\sim 3$  km/h), when the drifter escaped from the CA5 eddy and was carried away by the FC toward the Atlantic Ocean. The entrapment of the drifter inside the CubAN showed that the eddy's anticyclonic currents range between 0.2 m/s ( $\sim 0.5$  km/h) and 0.5 m/s ( $\sim 2$  km/h), being significantly smaller than the currents of the extended LC, which may reach the level of 1.5 m/s ( $\sim 5$  km/h). However, the currents due to the CubAN are still significant, especially within the narrow northern Cuba shelf.

For the calculation of relative vorticity, we used the drifter trajectory analysis software developed by Lilly et al. (2011). This tool is based on the use of a Morse wavelet decomposition to isolate and characterize the section of the trajectory during which the drifter is looping. This looping motion is analyzed in terms of a succession of time-varying ellipses, which allows estimating parameters of the looping trajectory, especially the size of the loops and the velocity of the drifter along them. This tool has already been used in the GoM to analyze the characteristics of a cyclonic LCFE (Le Hénaff et al., 2014). For the present trajectory, this analysis is able to isolate the section of the trajectory associated with the drifter looping, and to estimate ellipses representing this looping behavior (Figure A1c). In the hypothesis of a solid-body rotation, the angular velocity  $\Omega$  is constant, so that the velocity  $V$  inside the eddy is proportional to the distance  $R$  from the eddy center:  $V = \Omega \times R$ . In addition, the relative vorticity  $\zeta$  is also constant, equal to twice the angular velocity:  $\zeta = 2\Omega = 2V/R$ . Solid-body rotation has been observed for cyclonic eddies inside the GoM (Hamilton et al., 2002; Le Hénaff et al., 2014; Rudnick et al., 2015) and, in the neighboring Caribbean Sea, for North Brazil Current anticyclonic rings (Castelão & Johns, 2011). For the CubAN anticyclonic eddy sampled by drifter #70325, the estimates of the radius and velocity along the looping trajectory (Figure A1d) show that, in the hypothesis of a solid-body rotation, the relative vorticity of the CubAN eddy lies between  $\zeta_1 = -0.18 f$  ( $f$  the planetary vorticity), reached during the first loop within the CubAN eddy, and  $\zeta_2 = -0.12 f$  during the second loop; the angular velocities corresponding to  $\zeta_1$  and  $\zeta_2$  are indicated on Figure A1d. Although the velocity-radius profile suggests a decrease in relative vorticity from the first loop to the second one, the number of samples within the eddy, which form less than two complete loops, is too limited to conclude about a change in the relative vorticity of the observed CubAN. However, the order of magnitude of the relative vorticity for this anticyclonic eddy is robust and shows values between  $-0.1 f$  and  $-0.2 f$ ; this gives a measure of the CubAN's dynamical structure. More data are necessary at this stage to confirm the solid-body rotation within CubAN eddies, and to further assess the evolution of their vorticity signature during their advection along the Cuban coasts.

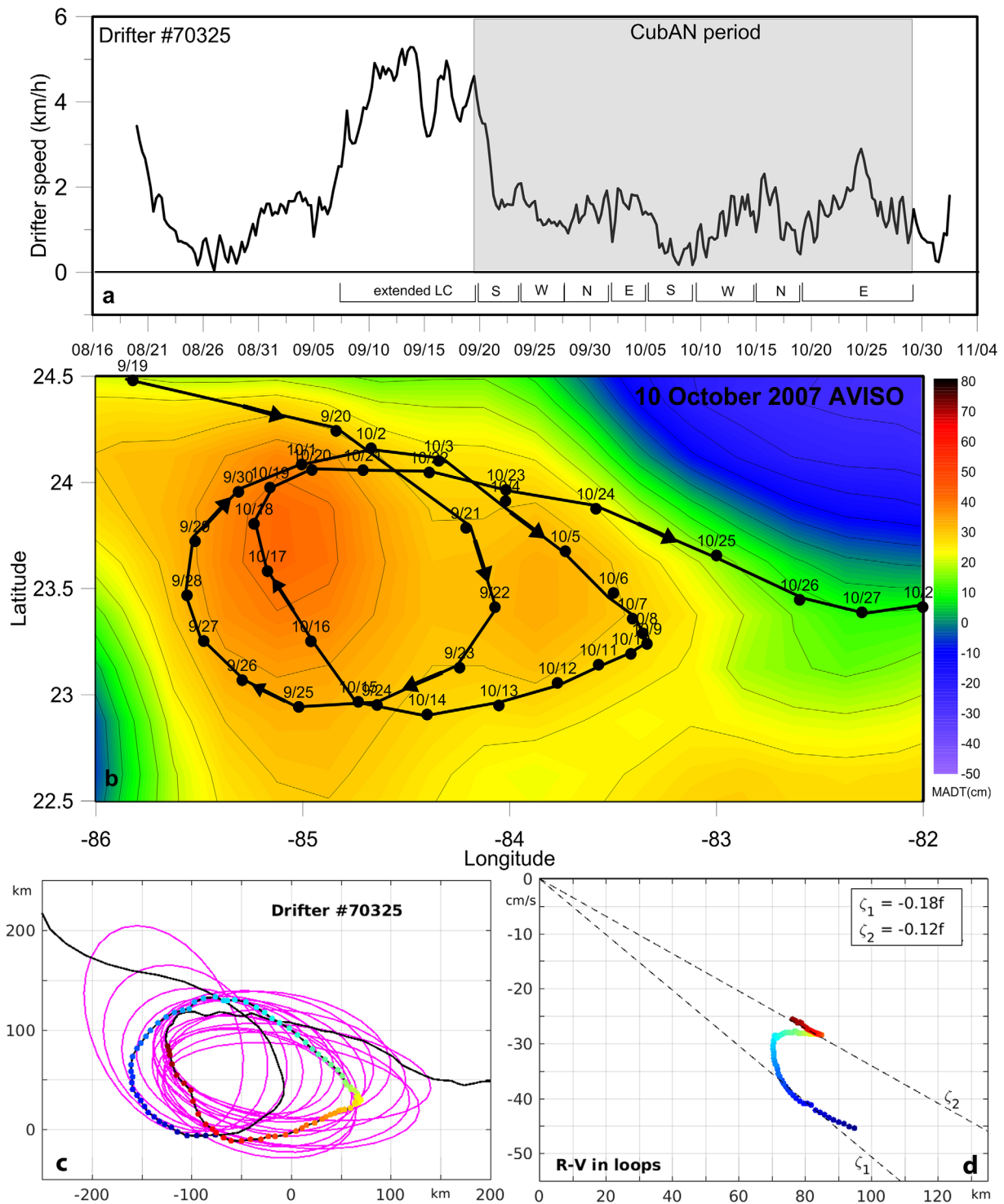


**Figure A1.** Analyses related to drifter #70325. (a) Evolution of 6-hourly speed (km/h); indications of the extended Loop Current (LC) and the main direction within the CubAN are given under the time series (S: southward, W: westward, N: northward, and E: eastward). (b) Daily locations during the drifter entrainment within a CubAN (CA5) in fall of 2007 (Case #3) (grey shaded area in Figure A1a) and horizontal distribution of AVISO Mean Absolute Dynamic Topography (MADT) on 10 October 2007. (c) Drifter trajectory (black line) in distance frame (km, centered on  $-83^\circ\text{W}$ ,  $23^\circ\text{N}$ ), with the location, in color, of the points for which the analysis tool identified a looping trajectory; the corresponding time-varying ellipses are in magenta. (d) Drifter velocity  $V$  (cm/s) along the looping trajectory (negative values for clockwise rotation), with the corresponding radius  $R$  values (km); the colors correspond to the color of the points identified on Figure A1; the minimum and maximum relative vorticity  $\zeta_1$  and  $\zeta_2$  along the looping trajectory under the hypothesis of solid-body rotation are indicated (see text for more details on the analysis).

### Acknowledgments

This research was made possible in part by a grant from The Gulf of Mexico Research Initiative (award GOMA 23160700) and in part by the National Oceanic and Atmospheric Administration (NOAA) RESTORE Act Science Program under award NA15NOS4510226 to the University of Miami. M. Le Hénaff acknowledges partial support from the Physical Oceanography Division at NOAA's Atlantic Oceanographic and Meteorological Laboratory, AOML. The ADCP data were provided by field studies under NOAA's Center for Sponsored Coastal Ocean Research award NA11NOS4780045 to the University of Miami; data analysis by Ryan Smith (NOAA-AOML) is acknowledged. We extend gratitude to Chuanmin Hu (Optical Oceanography Laboratory, University of South Florida), who produced the high-resolution ocean chl *a* images from MODIS data, which are openly accessible from NASA: <https://oceancolor.gsfc.nasa.gov/>. The mapped altimetry (AVISO) products were produced by the Ssalto/Duacs multiresolution system and distributed by the Copernicus Marine and Environment Monitoring Service (CMEMS; <http://www.marine.copernicus.eu>). Global Drifter Program data are distributed by NOAA (<http://www.aoml.noaa.gov/phod/dac/index.php>). The MUR Global High-Resolution SST data set is distributed by NASA (<http://podaac.jpl.nasa.gov/dataset/JPL-L4UHfnd-GLOB-MUR>).

### References

- Androulidakis, Y. S., Kourafalou, V. H., & Le Hénaff, M. (2014). Influence of frontal cyclone evolution on the 2009 (Ekman) and 2010 (Franklin) Loop Current eddy detachment events. *Ocean Science*, *10*(6), 947–965.
- Berg, R. (2017). *Hurricane Hermine* (Tropical Storm Rep. AL092016). Miami, FL: National Hurricane Center. Retrieved from [http://www.nhc.noaa.gov/data/tcr/AL092016\\_Hermine.pdf](http://www.nhc.noaa.gov/data/tcr/AL092016_Hermine.pdf)
- Bleck, R. (2002). An oceanic general circulation model framed in hybrid isopycnic-Cartesian coordinates. *Ocean Modelling*, *4*(1), 55–88.
- Candela, J., Sheinbaum, J., Ochoa, J., Badan, A., & Leben, R. (2002). The potential vorticity flux through the Yucatan Channel and the Loop Current in the Gulf of Mexico. *Geophysical Research Letters*, *29*(22), 2059. <https://doi.org/10.1029/2002GL015587>
- Castelão, G. P., & Johns, W. E. (2011). Sea surface structure of North Brazil Current ring derived from shipboard and moored acoustic Doppler current profiler observations. *Journal of Geophysical Research*, *116*, C01010. <https://doi.org/10.1029/2010JC006575>
- Chassignet, E. P., Smith, L. T., Halliwell, G. R., & Bleck, R. (2003). North Atlantic simulations with the Hybrid Coordinate Ocean Model (HYCOM): Impact of the vertical coordinate choice, reference pressure, and thermobaricity. *Journal of Physical Oceanography*, *33*(12), 2504–2526.
- Chérubin, L. M., Morel, Y., & Chassignet, E. P. (2006). Loop current ring shedding: The formation of cyclones and the effect of topography. *Journal of Physical Oceanography*, *36*(4), 569–591.
- Chérubin, L. M., Sturges, W., & Chassignet, E. P. (2005). Deep flow variability in the vicinity of the Yucatan Straits from a high-resolution numerical simulation. *Journal of Geophysical Research*, *110*, C04009. <https://doi.org/10.1029/2004JC002280>
- Cummings, J. A. (2005). Operational multivariate ocean data assimilation. *Quarterly Journal of the Royal Meteorological Society*, *131*, 3583–3604. <https://doi.org/10.1256/qj.05.105>
- Daley, R. (1991). *Atmospheric data analysis* (457 pp.), Cambridge, UK: Cambridge University Press.
- Donlon, C. J., Casey, K. S., Robinson, I. S., Gentemann, C. L., Reynolds, R. W., Barton, I., . . . Poulter, D. (2009). The GODAE high-resolution sea surface temperature pilot project. *Oceanography*, *22*(3), 34–45.
- Dussurget, R., Biorl, F., Morrow, R., & De Mey, P. (2011). Fine resolution altimetry data for a regional application in the Bay of Biscay. *Marine Geodesy*, *34* (3–4), 447–476.
- Felton, C. S., Subrahmanyam, B., Murty, V. S. N., & Shriver, J. F. (2014). Estimation of the barrier layer thickness in the Indian Ocean using Aquarius Salinity. *Journal of Geophysical Research: Oceans*, *119*, 4200–4213. <https://doi.org/10.1002/2013JC009759>
- Frantoni, P. S., Lee, T. N., Podesta, G. P., & Muller-Karge, F. (1998). The influence of Loop Current perturbations on the formation and evolution of Tortugas eddies in the southern Straits of Florida. *Journal of Geophysical Research*, *103*(C11), 24759–24779.
- Gierach, M. M., Subrahmanyam, B., & Thoppil, P. G. (2009). Physical and biological responses to Hurricane Katrina (2005) in a 1/25 nested Gulf of Mexico HYCOM. *Journal of Marine Systems*, *78*(1), 168–179.
- Halliwell, G. R. (2004). Evaluation of vertical coordinate and vertical mixing algorithms in the HYbrid-Coordinate Ocean Model (HYCOM). *Ocean Modelling*, *7*(3), 285–322.
- Hamilton, P., Berger, T. J., & Johnson, W. (2002). On the structure and motions of cyclones in the northern Gulf of Mexico. *Journal of Geophysical Research*, *107*(C12), 3208. <https://doi.org/10.1029/1999JC000270>
- Hodur, R. M. (1997). The Naval Research Laboratory's coupled ocean/atmosphere mesoscale prediction system (COAMPS). *Monthly Weather Review*, *125*(7), 1414–1430.
- Hodur, R. M., Hong, X., Doyle, J. D., Pullen, J., Cummings, J., Martin, P., & Rennick, M. A. (2002). *The coupled ocean/atmosphere mesoscale prediction system (COAMPS)* (No. NRL/JA/7530/01/0200). Monterey, CA: Naval Research Laboratory.
- Hurlburt, H. E., & Thompson, J. D. (1980). A numerical study of Loop Current intrusions and eddy shedding. *Journal of Physical Oceanography*, *10*(10), 1611–1651.
- Johns, W. E., & Schott, F. (1987). Meandering and transport variations of the Florida Current. *Journal of Physical Oceanography*, *17*(8), 1128–1147.
- Kendall, M. (1975). *Multivariate analysis*. London, UK: Charles Griffin & Company Ltd.
- Kourafalou, V. H., & Kang, H. (2012). Florida Current meandering and evolution of cyclonic eddies along the Florida Keys Reef Tract: Are they interconnected? *Journal of Geophysical Research*, *117*, C05028. <https://doi.org/10.1029/2011JC007383>
- Kourafalou, V. H., Mey, P. D., Hénaff, M. L., Charria, G., Edwards, C. A., He, R., . . . Zhu, X. (2015a). Coastal Ocean Forecasting: System integration and validation. *Journal of Operational Oceanography*, *8*, s127–s146. <https://doi.org/10.1080/1755876X.2015.1022336>
- Kourafalou, V. H., Mey, P. D., Staneva, J., Ayoub, N., Barth, A., Chao, Y., . . . Weisberg, R. H. (2015b). Coastal Ocean Forecasting: Science foundation and user benefits. *Journal of Operational Oceanography*, *8*, s147–s167. <https://doi.org/10.1080/1755876X.2015.1022348>
- Kourafalou, V. H., Peng, G., Kang, H., Hogan, P. J., Smedstad, O. M., & Weisberg, R. H. (2009). Evaluation of Global Ocean Data Assimilation Experiment products on South Florida nested simulations with the Hybrid Coordinate Ocean Model. *Ocean Dynamics*, *59*(1), 47–66. <https://doi.org/10.1007/s10236-008-0160-7>
- Leben, R. R. (2005). Altimeter-derived Loop Current Metrics. In *Circulation in the Gulf of Mexico: Observations and models* (pp. 181–201). Washington, DC: American Geophysical Union.
- Lee, T. N. (1975). Florida Current spin-off eddies. *Deep Sea Research and Oceanographic Abstracts*, *22*, 753–765. [https://doi.org/10.1016/0011-7471\(75\)90080-7](https://doi.org/10.1016/0011-7471(75)90080-7)
- Lee, T. N., Leaman, K., Williams, E., Berger, T., & Atkinson, L. (1995). Florida Current meanders and gyre formation in the southern Straits of Florida. *Journal of Geophysical Research*, *100*(C5), 8607–8620.
- Le Hénaff, M., Kourafalou, V. H., Dussurget, R., & Lumpkin, R. (2014). Cyclonic activity in the eastern Gulf of Mexico: Characterization from along-track altimetry and in situ drifter trajectories. *Progress in Oceanography*, *120*, 120–138.
- Le Hénaff, M., Kourafalou, V. H., Morel, Y., & Srinivasan, A. (2012a). Simulating the dynamics and intensification of cyclonic Loop Current frontal eddies in the Gulf of Mexico. *Journal of Geophysical Research: Oceans*, *117*, C02034. <https://doi.org/10.1029/2011JC007279>
- Le Hénaff, M., Kourafalou, V. H., Paris, C. B., Helgers, J., Aman, Z. M., Hogan, P. J., & Srinivasan, A. (2012b). Surface evolution of the Deepwater Horizon oil spill patch: Combined effects of circulation and wind-induced drift. *Environmental Science & Technology*, *46*(13), 7267–7273.
- Lilly, J. M., Scott, R. K., & Olhede, S. C. (2011). Extracting waves and vortices from Lagrangian trajectories. *Geophysical Research Letters*, *38*, L23605. <https://doi.org/10.1029/2011GL049727>
- Lumpkin, R., & Pazos, M. (2007). *Measuring surface currents with surface velocity program drifters: The instrument, its data, and some recent results*. Cambridge, UK: Cambridge University Press.
- Mann, H. B. (1945). Nonparametric tests against trend. *Econometrica: Journal of the Econometric Society*, *13*, 245–259.
- Mariano, A. J., Kourafalou, V. H., Srinivasan, A., Kang, H., Halliwell, G. R., Ryan, E. H., & Roffer, M. (2011). On the modeling of the 2010 Gulf of Mexico oil spill. *Dynamics of Atmospheres and Oceans*, *52*(1), 322–340.

- Metzger, E. J., Wallcraft, A. J., Posey, P. G., Smedstad, O. M., & Franklin, D. S. (2013). *The Switchover from NOGAPS to NAVGEM 1.1 Atmospheric Forcing in GOMS and ACNFS* (Tech. Rep. NRL/MR/7320 13-9486). Hancock, MS: Naval Research Laboratory, Stennis Space Center.
- Mezić, I., Loire, S., Fonoberov, V. A., & Hogan, P. (2010). A new mixing diagnostic and Gulf oil spill movement. *Science*, 330(6003), 486–489.
- Niiler, P. P., & Paduan, J. D. (1995). Wind-driven motions in the northeast Pacific as measured by Lagrangian drifters. *Journal of Physical Oceanography*, 25(11), 2819–2830.
- Oey, L. Y. (2004). Vorticity flux through the Yucatan Channel and Loop Current variability in the Gulf of Mexico. *Journal of Geophysical Research*, 109, C10004. <https://doi.org/10.1029/2004JC002400>
- Oey, L.-Y., Ezer, T., & Lee, H.-C. (2005). Loop Current, rings and related circulation in the Gulf of Mexico: A review of numerical models and future challenges. In W. Sturges & A. Lugo-Fernandez (Eds.), *Circulation in the Gulf of Mexico: Observations and models, Geophysical Monograph Series* (Vol. 161, pp. 31–56). Washington, DC: American Geophysical Union. <https://doi.org/10.1029/161GM04>
- Oey, L. Y., Lee, H. C., & Schmitz, W. J. (2003). Effects of winds and Caribbean eddies on the frequency of Loop Current eddy shedding: A numerical model study. *Journal of Geophysical Research*, 108(C10), 3324. <https://doi.org/10.1029/2002JC001698>
- Paris, C. B., Hénaff, M. L., Aman, Z. M., Subramaniam, A., Helgers, J., Wang, D. P., . . . Srinivasan, A. (2012). Evolution of the Macondo well blowout: Simulating the effects of the circulation and synthetic dispersants on the subsea oil transport. *Environmental Science & Technology*, 46(24), 13293–13302.
- Prasad, T. G., & Hogan, P. J. (2007). Upper-ocean response to Hurricane Ivan in a 1/25° nested Gulf of Mexico HYCOM. *Journal of Geophysical Research*, 112, C04013. <https://doi.org/10.1029/2006JC003695>
- Reverdin, G., Niiler, P. P., & Valdimarsson, H. (2003). North Atlantic Ocean surface currents. *Journal of Geophysical Research*, 108(C1), 3002. <https://doi.org/10.1029/2001JC001020>
- Roblou, L., Lamouroux, J., Bouffard, J., Lyard, F., Le Hénaff, M., Lombard, A., . . . Birol, F. (2011). Post-processing altimeter data towards coastal applications and integration into coastal models. In *Coastal altimetry* (pp. 217–246). Berlin, Germany: Springer.
- Rossov, V. V., & Santana, E. (1966). The hydrological researches of Soviet-Cuban expedition. In *Investigations of the central American seas* [Translated from Russian, 1973, U.S. Department of Commerce, Cat# TT70-57762] (pp. 1–24).
- Rudnick, D. L., Gopalakrishnan, G., & Cornuelle, B. D. (2015). Cyclonic eddies in the Gulf of Mexico: Observations by underwater gliders and simulations by numerical model. *Journal of Physical Oceanography*, 45(1), 313–326.
- Schmitz, W. J. (2005). Cyclones and westward propagation in the shedding of anticyclonic rings from the Loop Current. In *Circulation in the Gulf of Mexico: Observations and models* (pp. 241–261). Washington, DC: American Geophysical Union.
- Schott, F. A., Lee, T. N., & Zantopp, R. (1988). Variability of structure and transport of the Florida Current in the period range of days to seasonal. *Journal of Physical Oceanography*, 18(9), 1209–1230.
- Shay, L. K., Martinez-Pedraza, J., Cook, T. M., Haus, B., & Weisberg, R. H. (2007). High-frequency radar mapping of surface currents using WERA. *Journal of Atmospheric and Oceanic Technology*, 24, 484–503. <https://doi.org/10.1175/JTECH1985.1>
- Sponaugle, S., Lee, T., Kourafalou, V., & Pinkard, D. (2005). Florida Current frontal eddies and the settlement of coral reef fishes. *Limnology and Oceanography*, 50(4), 1033–1048.
- Sponaugle, S., Paris, C., Walter, K. D., Kourafalou, V., & Alessandro, E. D. (2012). Observed and modeled larval settlement of a reef fish to the Florida Keys. *Marine Ecology Progress Series*, 453, 201–212.
- Srokosz, M. A., & Bryden, H. L. (2015). Observing the Atlantic meridional overturning circulation yields a decade of inevitable surprises. *Science*, 348(6241), 1255575. <https://doi.org/10.1126/science.1255575>
- Sturges, W., Evans, J. C., Welsh, S., & Holland, W. (1993). Separation of warm-core rings in the Gulf of Mexico. *Journal of Physical Oceanography*, 23(2), 250–268.
- U.S. and Cuba Memorandum of Understanding. (2015). *Cooperation in the conservation and management of Marine Protected Areas*. Retrieved from <http://sanctuaries.noaa.gov/about/us-cuba-mou-english.pdf>
- Valentine, D. L., Mezić, I., Mačević, S., Črnjarić-Žic, N., Ivić, S., Hogan, P. J., . . . Loire, S. (2012). Dynamic autoinoculation and the microbial ecology of a deep water hydrocarbon irruption. *Proceedings of the National Academy of Sciences of the United States of America*, 109(50), 20286–20291.
- Vaz, A. C., Paris, C. B., Olascoaga, M. J., Kourafalou, V. H., Kang, H., & Reed, J. K. (2016). The perfect storm: Match-mismatch of bio-physical events drives larval reef fish connectivity between Pulley Ridge mesophotic reef and the Florida Keys. *Continental Shelf Research*, 125, 136–146.
- Von Arx, W. S., Bumpus, D. F., & Richardson, W. S. (1955). On the fine-structure of the Gulf Stream front. *Deep Sea Research*, 3(1), 46–65.
- Zavala-Hidalgo, J., Morey, S. L., & O'Brien, J. J. (2003). Cyclonic eddies northeast of the Campeche Bank from altimetry data. *Journal of Physical Oceanography*, 33, 623–629.